The Exchange of Fine Sediment in Gravel-Bed Fluvial Systems

Brayden J. Schiller

Thesis submitted to the Faculty of the
Virginia Polytechnic Institute and State University
in partial fulfillment of the requirements for the degree of

Master of Science
in
Civil and Environmental Engineering

Kyle Strom, Chair
Erich Hester
Emmanuel Frimpong

May 7, 2024
Blacksburg, Virginia

Keywords: fine sediment transport, mud, entrainment, deposition, chubs

The Exchange of Fine Sediment in Gravel-Bed Fluvial Systems

Brayden J. Schiller

ABSTRACT

The presence of fine muddy sediment (grain size < 0.1 mm) in streams has many impacts on the fluvial system and those relying on it, both humans and aquatic biota. Previously, fine sediment was considered a washload and has been ignored in transport models. More recently, it has been treated as being transported once the surface gravel layer that stores it is able to be mobilized. We propose that the surface layer need not be mobilized in order for muddy sediment to travel through the fluvial system in a series of erosive and depositional events. Our first study uses a new *in situ* device to show how mud entrainment from immobile gravel beds behaves cohesionlessly and can be modeled using the framework of classic sand-based models modified to account for hiding effects present in the stream bed. It also provides a method to predict how deep into the surface layer of gravel entrainment of fine sediment will occur given flow and stream bed characteristics. The second study investigates the primary pathway that fine sediment is traveling to get captured within bluehead chub fish nests. It was determined that more deposition of mud occurred in the upstream half of the nest concluding that the primary pathway was hyporheic pumping through the nest. Capture efficiencies of the nests were also found to increase as the length of nests increased. Both of these studies provide supporting evidence in the need to transition modeling fine sediment transport as a series of deposition and resuspension.

The Exchange of Fine Sediment in Gravel-Bed Fluvial Systems

Brayden J. Schiller

GENERAL AUDIENCE ABSTRACT

Fine muddy sediment (grain size < 0.1 mm) is present in natural streams and has many impacts on the stream system and those relying on it, including humans, plants, animals, and other organisms in the ecosystem. Previously, fine sediment was treated as being too small to consider in models that aid in understanding how a stream transports sediment. This is because small sediment stays suspended in the water column more easily than larger sediment. Therefore, it was just assumed to pass through the system and never deposit into the stream bed. However, in nature we observe large quantities of fine sediment being stored within the stream bed. More recently, it has been assumed that the sediment that does deposit will be transported once the surface gravel layer that stores it is able to be mobilized. That is, the surface gravel layer shields the fine sediment trapped between it and that the mud will stay put until that gravel is moved. We propose that the surface layer need not be mobilized for muddy sediment to travel through the fluvial system in a series of erosive and depositional events. Our first study uses a new device that forces erosion of mud to show how mud entrainment, or the process of how a fluid picks something up and carries it, from immobile gravel beds can be modeled using the framework of classic sand-based entrainment models modified to account for hiding effects, or protection against entrainment of a smaller sediment by a larger sediment shielding it, present in the stream bed. It also provides a method to predict how deep into the surface layer of gravel that fine sediment will be eroded given flow and stream bed characteristics. This is beneficial in estimating the amount of sediment that will be eroded during a given storm event. The second study investigates the primary pathway that fine sediment is traveling to get captured within bluehead chub gravel fish nests used for spawning their eggs and reproducing. It was determined that more deposition of mud occurred in the upstream half of the nest. This leads us to believe that the primary pathway of sediment traveling through the nest was hyporheic pumping through the nest, or the process of water flowing down through the surface layers of sediment in the stream bed. Capture efficiencies, or the ratio of how much of the sediment that traveled through the nest was captured, of the nests were also found to increase as the length of nests in the downstream direction increased. Both of these studies provide supporting evidence in the need to transition modeling fine sediment transport as a series of deposition and resuspension.

Acknowledgments

First I would like to thank my advisor, Kyle Strom, for this opportunity, along with everyone in my amazing research group for the constant support throughout this process. Thank you to Lailee DeLay, Sam Kraus, Jared Allen, Eric Hernandez, Angelina Passarelli, Shan Askari, Olivia Magenbauer, Thomas Bustamante, and anyone else who accompanied me into the field to collect data. Thank you to all my friends and family that I have made that have encouraged me along the way and provided emotional support when needed throughout graduate school. I could not have done this without any of these people. Thank you to Paolo Scardina for encouraging me to pursue a graduate degree and making it possible by offering me an assistantship and, furthermore, pushing me to do research. Thank you to all who provided me funding and financial support to make grad school possible for me including the Via fellowship, the U.S. Department of Energy under award number DE-SC0021402, and the National Science Foundation through grant IOS-2039692. Thank you to my parents for supporting me in everything that I do. Your support means the world to me. Thank you to the random people I met in coffee shops that allowed me to share my research with them even if they had no idea what I was saying. Thank you to the people at the Blacksburg Church of Christ for always supporting me. And thank you God for this incredible journey.

Contents

List of Figures

List of Tables

Chapter 1

Introduction

Fine muddy sediment (grain size < 0.1 mm) is a natural product of earth-surface processes that is generated in, delivered to, and transported through the fluvial system. This fine muddy sediment can be found in stream beds, floodplains, and in suspension from the system's mountainous regions down to coastal distributary deltas and bays, continental shelves, and deep ocean basins. Natural muddy sediment can be comprised of a large range of particle sizes and types. Mud can contain inorganic solid particles in the very-fine sand, silt, and clay range, organic material such as plant and animal detritus, bacteria, and their byproducts, or aggregates known as flocs that can be a mixture of all of these constituent particles (Shakeel et al., 2022).

Due to the small size of the particles, fine sediment of this size typically travels through streams and rivers suspended in the water column, i.e., it travels as suspended sediment load. In fact, particles smaller than 0.0625 mm have historically been considered to be a type of washload, which is when the sediment is too small to be captured or maintained within the system (Woo et al., 1986; Partheniades, 1977). In other words, the transport competence of the stream is too great for sediment this small to deposit within the system. Therefore, it is assumed that washload sediment will stay in suspension through the system until it exits into a slower, near-zero velocity region such as a lake, estuary, behind a dam, etc.

Though much of the fine muddy sediment traveling through the fluvial system will indeed eventually find its way to longer-term storage in near-zero velocity regions, the assumption that all fines will stay in suspension through the entire system as washload is an oversimplification that can significantly misrepresent reality. Many gravel and sand river beds contain fine muddy sediment (Dubuis and De Cesare, 2023). The fact that fine sediment can be considered a stream pollutant (Gupta et al., 2023) further highlights the fact that fine muddy sediment can deposit and erode from stream beds as it makes its way through the system.

Fine sediment is a natural product of earth-surface processes, but anthropogenic changes to the earth can further increase the supply or delivery of this fine material to streams. Higher intensity precipitation events coupled with constant land-use change drive up peak discharge and cause erosion of stream banks that often contain large fractions of fine sediment (Lane et al., 2019; Wharton et al., 2017). Human-caused climate change has increased sediment fluxes not only by higher intensity precipitation events but by glacier-snow permafrost melting as well (Li et al., 2020). This has a large effect on greater fine sediment fluxes. Additionally, increases in wildfire frequency surrounding fluvial systems contribute to increases in fine sediment supply and fluxes after hillslopes are burned and vegetation is

lost (Estrany et al., 2016).

The presence of fine sediment can be considered beneficial to society for the purposes of land building near coastal regions experiencing land loss in the face of sea level rise or subsidence (Blum et al., 2023). However, its presence in streams can also adversely impact both humans and the aquatic ecosystem surrounding the fluvial environment. For example, fine sediments that deposit in reservoirs deplete the reservoir's overall capacity and ability to provide flood protection and drinking or irrigation water during the summer seasons or droughts (Gupta et al., 2023). Suspended fine sediment in rivers or reservoirs can also pose a threat if the water is being used for potable water. In such situations, the filtration process becomes more expensive and there is a higher risk of increased bacterial aerobic spore concentrations entering the distribution systems on the suspended fines (Gauthier et al., 2003). Furthermore, sunlight needed by aquatic organisms on stream beds (including plants, algae, or invertebrates) reduces with increased turbidity brought on by increases in suspended fine sediment. Aquatic biota also gets affected by the duration that it is exposed to the suspended sediment (Newcombe and Macdonald, 1991). Fine sediment can also deposit in the coarse surface layer of gravel bed streams, thereby clogging the pore space (Frostick et al., 1984) and harming the organisms that live in the stream bed, including invertebrates and species that use the stream bed to spawn their eggs such as salmonid fish species (Bilotta and Brazier, 2008; Jensen et al., 2009).

For these reasons, it is necessary to understand how fine muddy sediment moves through the fluvial system and to find ways to account for its erosion, transport, and deposition in modeling frameworks. An assumption underlying this thesis work is that mud should not be considered a type of washload that bypasses the bed without depositing. Instead, mud should be envisioned as making its way through the system in a series of depositional and erosive events. This is especially true in gravel-bed streams where there is a large and diverse aquatic biota that lives and utilizes the pore space of the stream bed. Therefore, it is necessary to understand the deposition and erosion processes of fine sediment in gravel-bed streams, and this thesis focuses on doing so using *in situ* methods for measuring deposition and erosion in two gravel-bed stream configurations. The primary body of the thesis is presented in the following two chapters (Chapter 3 and 2) organized by study type. Each of the two chapters is presented as a stand-alone study with its own literature review, methods, results, discussion, and conclusion.

Chapter 2 presents a new, *in situ* method for measuring fine sediment erosion in aquatic systems. The method is then used to collect data on mud entrainment rates from stable gravel beds. Data collected are then used to test how historic entrainment equations, developed for sand-bedded rivers, perform when applied to predicting the entrainment of mud from stable, coarse surface-layer gravel. Adjustments to these models are also developed to provide a higher level of accuracy for the modeling fine sediment entrainment.

Chapter 3 examines depositional aspects of fine sediment transport within the particular context of siltation of Bluehead Chub fish nests. In the study, artificial nests are deployed in a local creek to measure the depositional patterns throughout the nest. The data is used to gain a stronger understanding of the depositional pathways and factors impacting the fine

sediment capture efficiencies of the nests.

The last chapter of the thesis summarizes the findings of both studies and their implication for understanding and modeling mud movement through the fluvial system.

Chapter 2

Entrainment of Fine Muddy Sediment from Plane Gravel Beds

2.1 Introduction

Sediment particles in rivers come in many different sizes, ranging from small clay particles that are approximately a micron in diameter up to large boulders whose diameters are on the order of meters. Predicting the movement of this vast range of particle sizes is difficult. Most riverbeds are dominated by sand (sediment in the size range of 0.065 to 2 mm) or gravel (a general term used here to encompass all sediment larger than 4 mm in diameter) (García, 2008). Because of this, most methods for predicting the transport, deposition, and erosion of sediment through the fluvial system have focused on predicting the movement of sand and gravel. Often, the finer "mud" fraction, consisting of a mixture of mineral and organic particles less than 62.5 μm (i.e., the silt and clay sizes), has been designated as wash load Woo et al. (1986). As such, mud is often conceptualized as a passive scalar that sees little interaction with the bed and instead travels through the system to deposit in low-velocity floodplains, ponds, lakes, reservoirs, and coastal estuaries and bays. However, river segments should not be thought of as complete bypass channels for mud. Instead, much like sand, we argue that suspended mud can go through multiple cycles of deposition and resuspension within the channel as the mud makes its way downstream.

For example, it has been shown in laboratory settings that even very fine sediment such as clays can deposit within a surface layer of gravel under conditions for which the shear velocity is much greater than the settling velocity of the sediment (Krishnappan and Engel, 2006; Mooneyham and Strom, 2018a) and that the rate of loss of suspended clays to the bed is a function of the pore Reynolds number (Fries and Trowbridge, 2003; Mooneyham and Strom, 2018a). Pumping of surface water through sandy dunes can also lead to the trapping of clay within the bed (Packman et al., 2000). This trapped clay then can mix with the sand and produce alterations in the morphology and dynamics of the bedforms (Dallmann et al., 2020, 2021). Furthermore, in the field, Skalak and Pizzuto (2010) have observed significant quantities of mud that they estimate has storage time scales on the order of decades along the channel margins and behind woody debris in a gravel bed stream within an agricultural watershed in Virginia. And, Buendia et al. (2016) found that suspended sediment concentrations following storm events were larger when there was a larger volume of fines stored in the bed prior to the flood event (Buendia et al., 2016).

These studies and examples all point to the need to conceptualize the river bed as a

transient storage zone for fine muddy sediment making its way downstream. While this process of storage and release of mud can be conceptualized, a standard method of modeling mud transport through sand and gravel rivers remains unrealized. A contributing reason for this unrealized ability to model mud in such situations is that boundary exchange fluxes (i.e., deposition and entrainment flux) for muddy suspensions flowing over different bed types are not fully understood. This research aims to expand our ability to model the movement of mud through gravel-bed rivers by studying the entrainment of mud from immobile gravel beds.

2.2 Background

Suspended sediment movement in a 1D river framework can be modeled using the 1D advection-diffusion equation.

$$\frac{\partial(AC_v)}{\partial t} + \frac{\partial(AUC_v)}{\partial x} = \frac{\partial}{\partial x}\left(AD_c\frac{\partial C_v}{\partial x}\right) + b(E - D) \tag{2.1}$$

where A is the cross-sectional flow area, C_v is the suspended sediment concentration in terms of a volume fraction, U is the cross-sectionally averaged velocity, D_c is the dispersion coefficient, and E and D are erosional and depositional sediment volume fluxes into and out of the bed. Typically, D is modeled as the product of settling velocity, w_s, and C_v, $D = w_s C_v$, and with E being modeled as,

$$E = w_s E_s \tag{2.2}$$

Here E_s is a non-dimensional entrainment coefficient. Note that a mass entrainment flux can be defined as,

$$E_M = \rho_s E \tag{2.3}$$

where ρ_s is the density of the sediment being entrained.

In a 1D framework, the hydraulic quantities $U = U(x,t)$ and $A = A(x,t)$ can be used along with equation 2.1 to model the movement of suspended sediment if w_s and E_s can be defined. w_s is constrained by the size and density of the sediment being modeled (García, 2008), and E_s is typically calculated with entrainment closure equations such as the ones proposed by Smith and McLean (1977), van Rijn (1984), or Garcia and Parker (1991); for an expanded list of model options for E_s see (García, 2008). Equation 2.1 could also be used to track the movement and storage of mud throughout a river if the equation is coupled with a conservation equation for the mud stored in the bed.

All models for E_s, that we are aware of, were created with sand transport in mind. The theory and data used to develop the equations assume a bed uniformly covered with sand. In addition, the empirical data used in the development of the model typically came from experiments in which equilibrium conditions prevailed, i.e., there were no temporal or longitudinal gradients in C_v, U, or A, implying that entrainment and deposition must be balanced (equation 2.1). As such, E_s was taken to be equal to the measured concentration.

One distinction between mud and non-cohesive sands and gravels is that individual mineral and organic mud particles can stick together or aggregate into larger particles known as "flocs", thereby altering the settling speed and depositional flux of the flocculated suspension relative to that of unflocculated mud (Mehta, 2022). Therefore, mud deposition flux should be modeled with the settling velocity of the flocs (e.g., Strom and Keyvani, 2011) rather than the settling velocity of the unaggregated mud. Furthermore, large build-ups of mud in the bed can possess a level of cohesion that adds additional resistance over that of simple particle weight working against erosion. For these reasons, the entrainment flux of mud has historically been calculated as:

$$E_M = \alpha(\tau - \tau_c)^\beta \tag{2.4}$$

where α and β are fit coefficients, τ is the bed shear stress, and τ_c is the bed shear stress at which erosion of the cohesive mud bed commences, i.e., the critical value, and is typically taken to be a function of depth due to consolidation (e.g., Sanford and Maa, 2001; Mehta, 2022). This modeling approach is used when the bed is composed solely of mud (e.g., an estuary or bay), and β, α, and τ_c are all taken to be site-specific parameters that must be determined through experimentation (e.g., Wiberg et al., 2013). This approach to cohesive erosion assumes that any material eroded from the bed is immediately entrained into suspension, and it does not consider any individual particle or floc properties.

One study that has sought to model the storage and release of fine particles in a gravel bed river is that of Park and Hunt (2018). Park and Hunt (2018) took a simplified approach to the model and assumed that the system was purely depositional when the flow competence was lower than that required to mobilize the bed. That is, they took $E = 0$ for the fine particles up until the gravel was mobilized. When the flow competence was great enough to mobilize the gravel, then the fines that had been stored in the gravel were released in a pulse back to suspension. Under such a condition, E is taken to be a function of the volume of fines stored within the pore space of the surface layer and the τ_c value of the gravel. This approach of limiting the entrainment of fines until the gravel surface layer is mobilized is in line with the suggestions and findings of Harvey et al. (2012) and Mooneyham and Strom (2018a).

2.3 Research Questions and Hypotheses

In this research, we seek to answer three related questions. The first is, can mud entrain into suspension from a gravel bed before the gravel surface layer is mobilized? While it is reasonable that the breakup of the surface layer will release the fine sediment stored below the surface of these grains, we hypothesize that entrainment of mud out of a gravel surface layer is possible without the mobilization of the surface-layer stones (H1). Therefore we expect that mud can go through multiple cycles of deposition and entrainment with more frequent flow events that sit below the typical bankfull condition needed to mobilize the gravel surface layer.

The second question this study seeks to answer is, do historic entrainment equations

developed for and with data from sand-bed channels work to predict the entrainment rate of mud from the surface of a gravel bed stream? In many gravel-bed streams that we have waded in, we have observed that mud that has settled to the surface layer or pore space of the stream is often visually flocculated and loosely stored (i.e., cohesion appears to be minimal due to the ease at which the material enters suspension when walking through a stream). The existence of a loose muddy layer composed of large flocculated material that behaves cohesionlessly with respect to other flocculated mud in the bed is also in line with the work of Schieber and Southard (2009) and Tran and Strom (2019). Therefore, we propose that a reasonable approach to modeling mud movement in such streams is to treat the mud as a low-density, cohesionless material. Based on this assumption, we expect that entrainment of the flocculated material could be described with models developed for cohesionless sediment rather than the classic cohesive mud erosion equation (equation 2.4). We specifically hypothesize that classic sand-based E_s models will produce incorrect entrainment values in their unaltered state, but that the form of the equations will provide a reasonable framework that can be adjusted to predict the entrainment of mud (H2).

Thirdly, we explore how entrainment of mud is modulated by the embeddedness of the gravel in the fine sediment. Embeddedness is a measure of how far up the fine sediment surrounding the gravel surface layer lies relative to the top of the gravel (Smith, 2023). If the gravel is 100% embedded, then the surface layer is entirely encased in mud and one would expect that the mud must erode before the gravel and that entrainment rates will be higher due to the larger surface area of the mud bed. If the embeddedness is 5%, then one would expect that the majority of the mud is hiding down in the protected pore space of the gravel, leading to lower entrainment values and possibly necessitating that the gravel must move before the mud can be released. The specific questions pertaining to the role of embeddedness on entrainment are, does the initial embeddedness influence the entrainment flux, and can the final embeddedness of the gravel be predicted (i.e., the state when entrainment ceases)? We hypothesize that the answer to both is "yes" (H3 and H4).

2.4 Methods

2.4.1 Overview

To test these hypotheses, we measure the mass erosion flux, E_M (equation 2.3), at nine different sites within three gravel-bed streams with different surface layer grain size distributions and levels of embeddedness and applied bed shear stress. We then compare the mobility of the mud and gravel to test H1. H2 is examined by putting the measured E_M values in terms of E_s and then comparing the measured E_s values to those predicted using the Smith and McLean (1977), van Rijn (1984), or Garcia and Parker (1991) entrainment equations (described below) and adjusting them as needed. H3 and H4 are tested using the measured entrainment values and the initial and final embeddedness for each run. A new erosional flume was designed and built as part of this work to provide a means by which the applied shear stress could be controlled in the field and the resulting E_M measured. The

new erosional flume, referred to as the Benthic Canon, is described below along with the field sites and experimental procedures.

2.4.2 Historic entrainment equations for sand

One classic model of E_s we wanted to test was that of Smith and McLean (1977):

$$E_s = \frac{0.65\gamma_0 T}{1 + \gamma_0 T} \tag{2.5}$$

where T is the scaled excess shear stress applied to the bed,

$$T = \frac{\tau^* - \tau_c^*}{\tau_c^*} \tag{2.6}$$

and γ_0 is a constant equal to 2.4×10^{-3}. In equation 2.6, τ^* is the non-dimensional bed shear stress, or Shield parameter, associated with the skin component of shear (or the shear responsible for moving sediment). The Shields parameter is defined as,

$$\tau^* = \frac{\tau}{\rho g R_s d} = \frac{u_*^2}{g R_s d} \tag{2.7}$$

τ_c^* is the critical Shields parameter (the value of τ^* when sediment grains just start to move). In the above, ρ is the density of water, g is the acceleration of gravity, and $R_s = (\rho_s - \rho)/\rho$ is the submerged specific gravity of the sediment whose density is ρ_s, and the d is the grain diameter. We note here the relationship between shear velocity and bed shear stress is:

$$u_* = \sqrt{\frac{\tau}{\rho}} \tag{2.8}$$

Equation 2.5 predicts the entrainment coefficient, or volume flux of entrained sediment scaled by the particle settling velocity (equation 2.2), as a function of the excess Shields stress.

Similarly, the van Rijn (1984) modeled entrainment coefficient with,

$$E_s = 0.015 \frac{d}{b} \frac{T^{1.5}}{D_*} \tag{2.9}$$

where b is the roughness length scale and D_* is a type of particle Reynolds number defined as,

$$D_* = d \left(\frac{R_s g}{\nu^2} \right)^{1/3} \tag{2.10}$$

Here ν is the kinematic viscosity of water. The van Rijn (1984) method for obtaining E_s (equation 2.9) requires the same input as that of Smith and McLean (1977) with the addition of the kinematic viscosity.

A third commonly used entrainment equation is that of Garcia and Parker (1991). Modifications to the original formulation have been proposed over the years for different situations (e.g., Garcia and Parker, 1993; Wright and Parker, 2004), but we here examine the original equation. The formulation includes many of the same base input values as equations 2.5 and 2.9, but the method presents E_s as a function of the following non-dimensional number, Z_u:

$$Z_u = \frac{u'_*}{w_s} R_p^{0.6} \tag{2.11}$$

with w_s being the settling velocity, u'_* the skin shear velocity applied to the bed and R_p the following Reynold's particle number:

$$R_p = \frac{du_g}{\nu} \tag{2.12}$$

where u_g is the grain velocity scale $u_g = \sqrt{dgR_s}$. E_s is calculated with the Garcia and Parker (1991) method as,

$$E_s = \frac{AZ_u^5}{1 + \frac{A}{0.3} Z_u^5} \tag{2.13}$$

with A being a constant equal to 1.3×10^{-7}.

To calculate E_s with any of these three equations (equations 2.5, 2.9, and 2.13), one must know the size of the sediment being entrained, d, the critical Shield value, τ_c^*, the applied skin friction shear stress, τ, or shear velocity, u_*, the density of the sediment, ρ_s, and the density and kinematic viscosity of the water, ρ and ν.

2.4.3 Erosional Flume

Critical to this study is the *in situ* measurement of E or E_M for different hydraulic and stream bed conditions. To do this, we designed and built a mobile erosional flume that could be installed in streams that exhibited mud in the surface layer and variation in the surface layer grain size distribution and embeddedness. This forced the need to collect measurements in slower velocity reaches on calm days not directly after a significant precipitation event. Reaches with slower velocities allowed for the aggregation of fine sediment within the bed and made it possible to install and secure the equipment. Since these slower velocity areas were targeted due to their ability to allow fine sediment to deposit and get trapped within the gravel bed, a device needed to be constructed with the ability to adjust and increase the flow velocity, and more specifically, the shear stress being applied to the bed.

The device, hereafter referred to as the Benthic Cannon or just the Cannon, consists of a 1.83 m long hard vinyl square duct with a 9.5 by 9.5 cm cross section and a fine-sediment filtering reservoir that holds two single-speed sump pumps that move water through the Benthic Cannon at a rate controlled by two ball valves. An optical backscatter sensor (OBS) and a velocity meter are used at the end of the Cannon to measure the exiting water turbidity and velocity.

The test section is a 30.5 cm by 8 cm rectangle that is removed from the bottom of the Benthic Cannon that starts 1.2 m down the 1.83 m duct and ends 0.3 m from the end of the Cannon. There is a plastic skirt constructed and attached surrounding the test section to ensure a better seal with the bed so that all eroded muddy material exits out the end of the Cannon and is recorded by the OBS rather than jetting out the bottom. A basic schematic of the Benthic Cannon system is shown in figure 2.1.

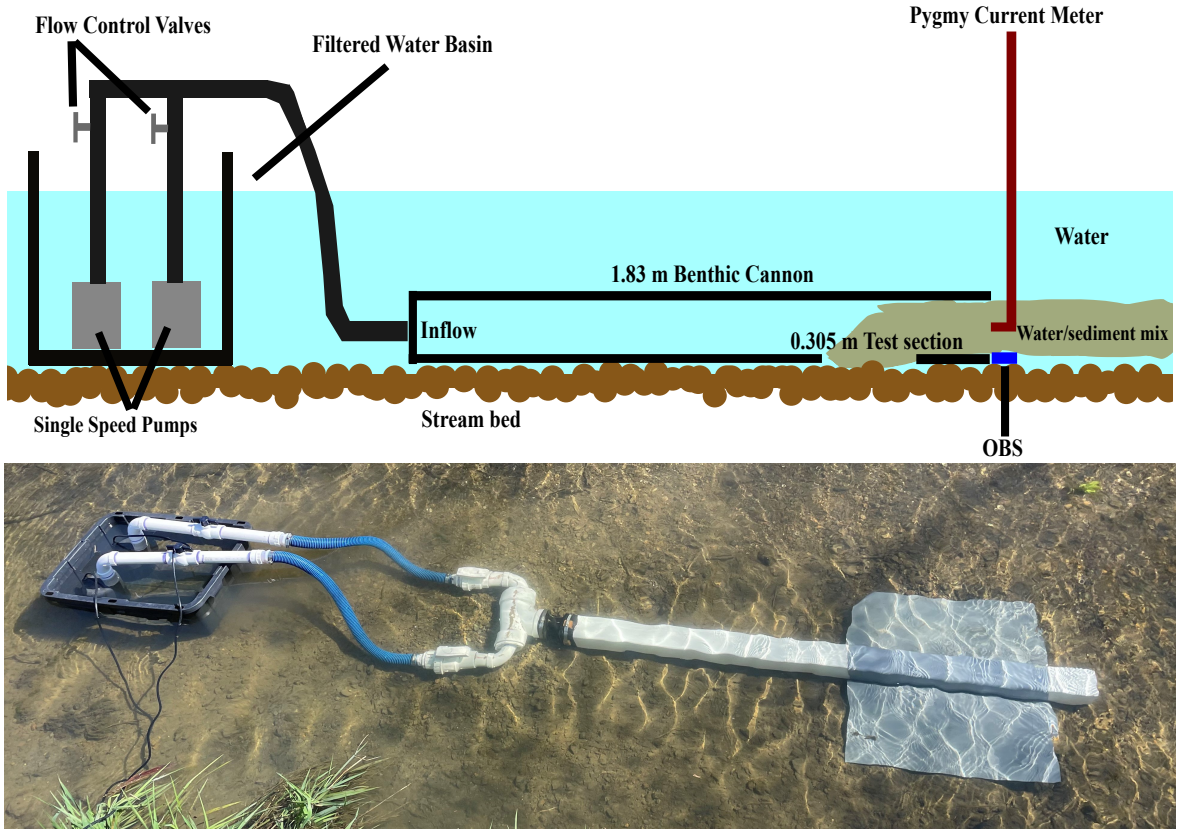

Figure 2.1: Schematic and image of the Benthic Cannon Apparatus used for entrainment testing

2.4.4 Study Sites

Erosion experiments were conducted at nine different locations; some sites were visited multiple times to conduct trials. All of the streams were located in southwest Virginia near the town of Blacksburg and had surface layers composed of gravel. It was important to vary the testing location to obtain a variety of parameter combinations. Sites were prioritized for different levels of embeddedness and d_{50} because shear stress was varied and controlled with the Benthic Cannon.

Limitations to the study area included the size of the gravel making up the bed, flow velocities of the stream section, and depth. The test section of the Benthic Cannon is only

8 cm wide. So the gravel cannot be too large to prohibit an adequate seal with the bed. In addition, swift-moving areas were avoided to evade difficulties in anchoring equipment to the stream bed. The testing sites must also have been greater than 10.5 cm in water depth to ensure that the Cannon was completely submerged, but not too deep as a vessel was not used for testing, so the streams must have been wadeable. The stream sites selected were chosen in both rural and urbanized areas where access to the stream could minimize the transport of equipment to the site. A map of the sites can be seen in figure 2.2.

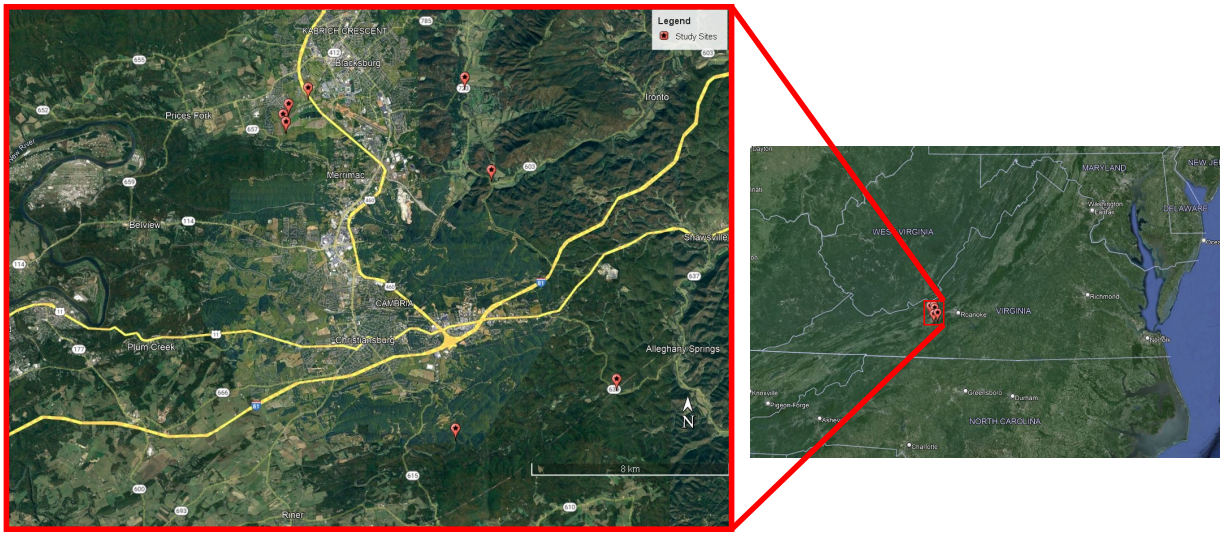

Figure 2.2: Map of locations used for entrainment testing

2.4.5 General Procedure

A location within each sample reach whose stream bed visually appeared to be uniform was chosen for each trial. For a testing location to be used, there needed to be at least four 31 cm by 8 cm sections of the bed that were similar to each other visually with gravel size and embeddedness levels.

Before measuring erosion with the Cannon, one section of the study area was used to measure the initial embeddedness of the location (section 2.4.7 discusses how embeddedness was measured). The Benthic Cannon was then placed in the stream with the test section opening on an identified sample section of the bed. After setting up the Cannon, the entire area was left undisturbed to allow any suspended fines that were stirred up by the installation process to settle or advect downstream before starting the erosion test. Following this, the pumps were turned on with the ball valves closed. The valves were then slowly opened until a suspension of fine sediment was seen exiting the Cannon. The flow velocity exiting the Cannon was then measured using a Pygmy Current Meter. This flow velocity was later converted to a shear velocity (see Section 2.4.8 for details) and labeled the "incipient shear velocity" of the site. Identification of the initiation of suspended sediment condition was a

purely visual designation because the OBS did not always pick up the very low, and not always well-mixed, conditions associated with the inception of mud entrainment.

For each subsequent trial, within the testing location, the Cannon was moved to the next adjacent test area of the bed. The pumps were again turned on with the ball valves closed and then slowly opened until just before the critical flow velocity where initiation of suspended sediment was observed. At this point, the valves were opened to increase the velocity in the Canon relative to the velocity of the previous trail. The slow initial opening of the valves was done to reduce the effect of an unsteady pulse of water on the entrainment of the mud as much as possible. Once the velocity was set, the pumps were left running until there was no visible suspended sediment exiting the end of the Cannon. Following this, the apparatus was moved and the resulting final embeddedness of the test section was measured. An example of an area of stream bed before and after a test was run is demonstrated in figure 2.3. Once the trials were concluded in a given test location, a large sample of the surface-layer gravel was collected for grain sizing.

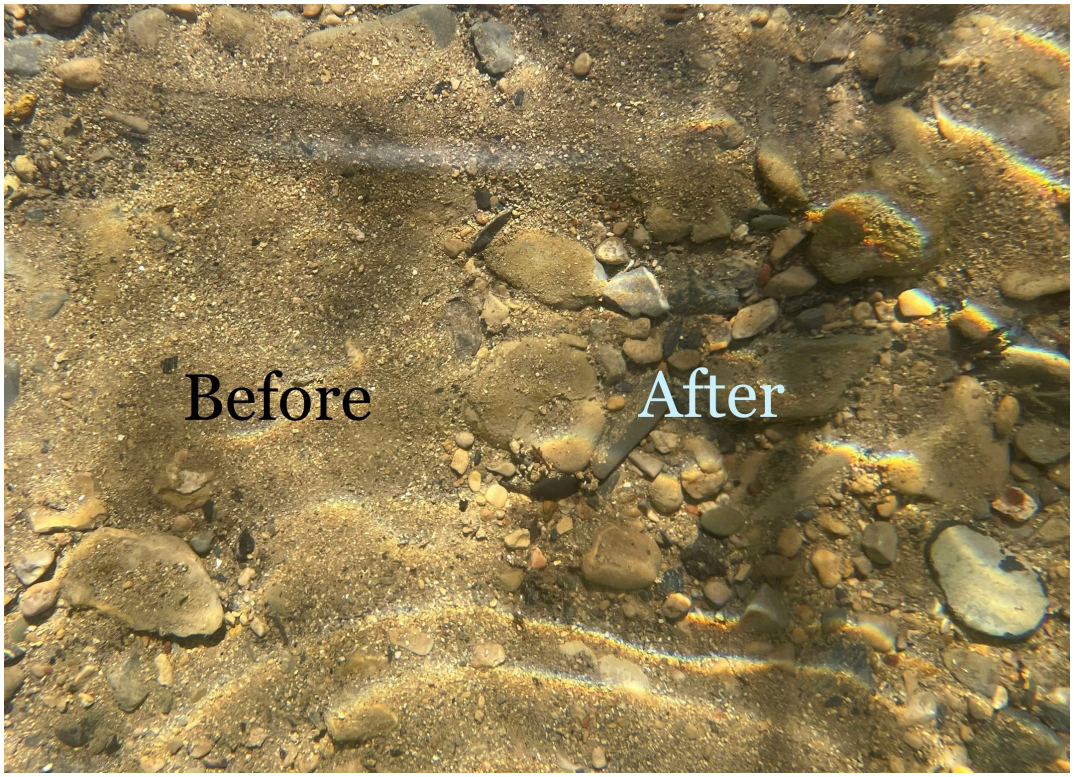

Figure 2.3: Stream bed fine sediment presence before and after an erosive test was performed to determine entrainment with the Benthic Cannon

2.4.6 Grain Size

A standard sieve analysis was conducted for each surface layer sample collected to obtain a grain size distribution and extract an average d_{50} of the gravel, or grain size in which 50 percent of the gravel is larger and 50 percent is smaller than the given size by weight. Samples of grain size distributions at the testing sites are shown in figure 2.4.

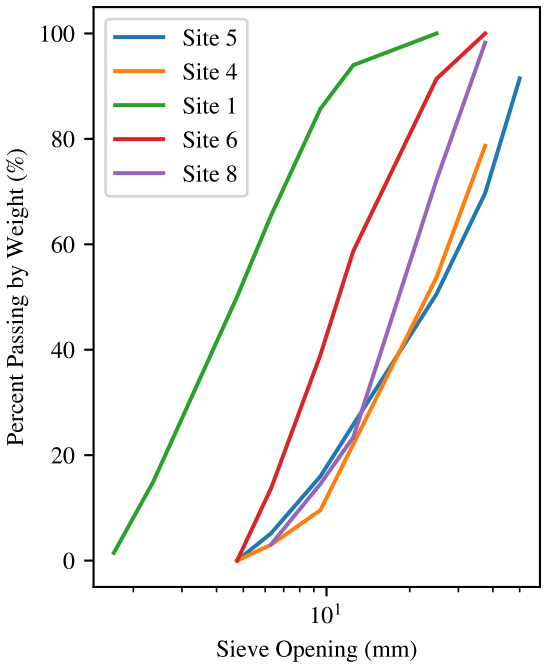

Figure 2.4: Sample grain size distributions of testing sites gravel surface layer

The field microscope known as the FlocARAZI (Osborn et al., 2021) was used to measure the size of the eroded mud. The FlocARAZI is an image-based system capable of *in situ* measurements of suspended solid and flocculated particles in the size range of 10 μm to 2 mm. In some of the tests, the FlocARAZI was placed at the exit of the Benthic Canon to capture the size of the muddy material being eroded. Figure 2.5 is a characteristic example image from one test. Particle sizes are measured automatically using a set of image-processing routines outlined in the following GitHub repository, `https://github.com/Floc-Imaging-and-Image-Processing/FlocCam-ImageProcessing`. The process identifies and measures the area of in-focus particles and uses the measured area, A_{pi} to extract a representative particle or floc diameter, $d_i = \sqrt{4A_{pi}/\pi}$, and volume, $V_{pi} = \pi d_i^3/6$. These particle measures of d_i and V_{pi} are then used to build particle size distributions and calculate size distribution statistics. Using the data from the FlocARAZI, average size statistics for the eroded mud were $d_{f16} = 48$ μm, $d_{f50} = 133$ μm, and $d_{f84} = 300$ μm.

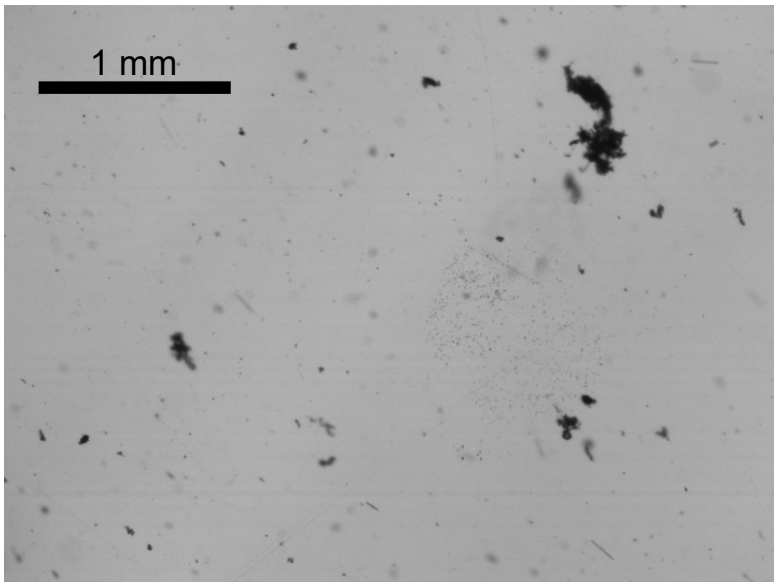

Figure 2.5: Muddy suspended sediment entrained by the Benthic Cannon and captured by the FlocARAZI

2.4.7 Embeddedness

Embeddedness, *emb*, is the measurement of how surrounded the surface layer gravel is by fine sediment (Smith, 2023). This is represented as a percentage of a piece of gravel that is buried under fine sediment. This measurement is made by grabbing a piece of gravel and marking with the tip of your thumb on the gravel where it is buried up to in fine sediment before lifting it off of the stream bed. The vertical distance from the bottom of the gravel to the point marked by the thumb, z, is measured first. Then the entire vertical height of the gravel, h, is measured. The embeddedness for an individual gravel grain is computed as

$$emb = \frac{z}{h} \times 100\% \tag{2.14}$$

The embeddedness of each location was measured at each testing location at an undisturbed area, the same size as the Benthic Cannon's testing section (30.5cm × 8cm), as the initial value. Then the resulting embeddedness of the test section was measured after each erosion test was conducted. Every piece of gravel that fell within the test section was measured for its embeddedness and the average of these values was computed to get a representative embeddedness value of the test section. If the gravel was completely buried in fines, the *emb* value for that gravel piece was 100 percent. Similarly, if it was fully exposed, the value was 0 percent. A minimum of 30 pieces of gravel were measured for each test section to ensure a valid representation of embeddedness was determined.

2.4.8 Shear Velocity

The shear velocity and shear stress the Cannon exerted on the bed during each trial were calculated using the measured flow velocity exiting the Cannon, U, and a Darcy-Weisbach friction factor, f, determined with the Colebrook equation. That is,

$$\tau = \rho \left(\frac{f}{8} \right) U^2 \tag{2.15}$$

where f is obtained using the Colebrook equation,

$$\frac{1}{\sqrt{f}} = -2 \log \left(\frac{\epsilon}{3.7 D_h} \right) + \frac{2.51}{Re\sqrt{f}} \tag{2.16}$$

In equation 2.16, D_h is the hydraulic diameter ($D_h = 4R_h$) where R_h is the hydraulic radius, and Re is Reynolds Number ($Re = 4R_h U/\nu$). The absolute roughness value of the smooth plastic pipes, ϵ, was assigned a value of 0.0015 mm. u_* and τ were related through equation 2.8. All shear stress experienced within the Cannon is assumed to be skin shear stress.

2.4.9 Mass Erosion Rates and Calculation of E_M and E_s

The rates of erosion produced by the Cannon were measured using the OBS attached to the RBR duo3 logger. The turbidity data was recorded in units of NTUs, which is a measurement of the opaqueness of the water, at a rate of 2 Hz. Having a sampling rate over 1 Hz was crucial because the erosion tests only take on the order of seconds to complete due to the small test section. Turbidity in NTUs can be linearly correlated to a suspended sediment concentration, C. A calibration between the two (NTUs and C in gr/L or kg/m^3) was developed in a well-mixed laboratory tank by adding a known mass of fine stream bed sediment to a known volume of water and recorded the turbidity with the same OBS sensor used in the field experiments. This calibration was done independently with mud samples from two different streams, but no meaningful difference was observed between the calibration equations. For this reason, all of the data were pooled to create a single calibration equation for all streams, $C = 0.0022(NTU) + 0.0056$ ($R^2 = 0.97$) where C is in kg/m^3.

After converting the data to C, the OBS data provides a mass concentration time series for each erosion trial. The mass flow rate exiting the cannon can be defined as,

$$\dot{M}(t) = \int_{A_c} uC(t) dA_c = U_c \langle C(t) \rangle A_c \tag{2.17}$$

where $\dot{M}$ is the mass flow rate, u is the steady velocity field within the cross-sectional flow area of the Canon, A_c, U_c is the cross-sectionally averaged velocity exiting the Cannon, and $\langle C(t) \rangle$ is the concentration spatially averaged over A_c. For our purposes, we assume that U is the velocity measured using the pygmy meter, and that $\langle C(t) \rangle = C(t)$ from the OBS measurements,i.e, the OBS sees the average concentration existing the cannon, or the suspension is well mixed over A_c.

Equation 2.17 produces a mass flow rate time series for each trial. Integrating $\dot{M}$ over time and subtracting off the mass associated with the background or base flow gives a total mass eroded from the test site during each trial. This was accomplished practically as,

$$M = \int_{\Delta t} \dot{M}(t)dt - \frac{\dot{M}(t_f) + \dot{M}(t_0)}{2}(\Delta t) \tag{2.18}$$

where

$$\Delta t = t_f - t_0 \tag{2.19}$$

with t_0 being the time at which the concentration initially begins to deviate from the baseflow condition, t_f being the time when the concentration time series returns to the baseflow condition (Figure 2.6). t_0 and t_f were identified manually for each trial.

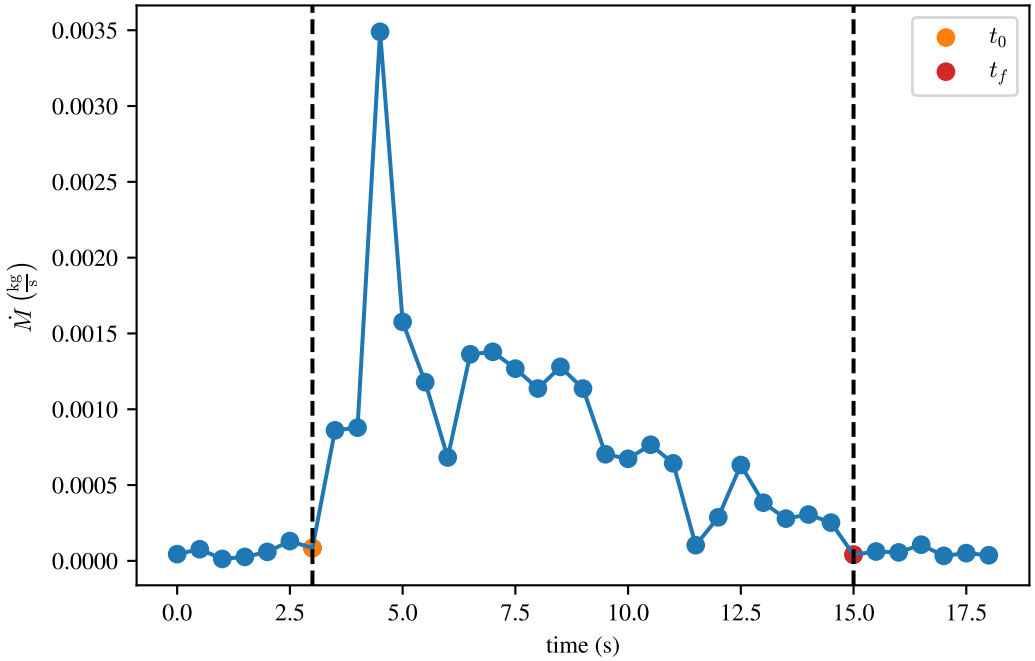

Figure 2.6: Identifying the initial and final time for integration of the mass flux time series obtained from the OBS turbidity data

The mass erosion rate, E_M, for each trial was obtained by dividing the total mass eroded during the trial by the time of the trial and the area of the bed test section, A_{TS}, in the Benthic Cannon:

$$E_M = \frac{M}{A_{TS}\Delta t} \tag{2.20}$$

This provides an erosive flux with units kg/(s-m^2) for each trial. E_s was then calculated for each trial according to equation 2.2 and 2.3 as,

$$E_s = \frac{E_M}{\rho_s w_s} \tag{2.21}$$

Because the material being eroded is mud, we use the floc size and fractal dimension, n_f, to define the sediment density and settling velocity as the floc density, ρ_f, and settling velocity. To do this, we used the following:

$$\rho_f = R_f \rho + \rho \tag{2.22}$$

where R_f is the floc submerged specific gravity,

$$R_f = R_s \left(\frac{d_f}{d_p} \right)^{n_f - 3} \tag{2.23}$$

d_f is the size of the flocs, d_p is the size of the particles making up the flocs, and n_f is the fractal dimension of the flocs.

The floc settling velocity was calculated using (Strom and Keyvani, 2011),

$$w_s = \frac{g R_f d_f^2}{b_1 \nu + b_2 \sqrt{g R_f d_f^3}} \tag{2.24}$$

with b_1, b_2, and n_f set to 100, 0, and 2.5 respectively following the recommendations of (Strom and Keyvani, 2011), and d_p was assumed to be 10 μm based on previous grain sizing of disaggregate stream mud from Stroubles Creek. Calculated ρ_f and w_s values were based on the measured d_{f50} values of 133 μm.

2.5 Results

2.5.1 Erosion Without Bed Mobilization

The largest shear velocity experienced in any of the trials was $u_* = 0.033$ m/s. Assuming that initiation of motion occurs between a Shield's parameter, τ^*, of 0.03 and 0.05, this shear velocity had the ability to mobilize gravel between 1 and 3 mm. This was determined using equations 2.8 and 2.7.

2.5.2 Parameter Effect on Erosion Rates

A multiple linear regression with independent variables as initial embeddedness, d_{50} of the gravel bed, and skin shear velocity applied to the bed and dependent variable being the erosive flux measured was conducted with a 95% confidence interval. The p-values associated with each variable can be located in table 2.2. We see that shear velocity has the greatest impact on the flux, followed by the bed gravel material size, and then the initial embeddedness. The initial embeddedness is the only variable that did not have a statistical significance.

Figure 2.7 shows the results from the linear regression and how well the independent variables together can predict erosion rates of fines from the stream bed.

Site	Stream	d_{50} (mm)	u_* Critical (m/s)	u_* Applied (m/s)	τ^*_{cr} mud (gravel)	τ^*/τ^*_{cr} mud (gravel)	emb_0 (%)	emb_f (%)	E_s (-)
1	Stroubles Creek	5	N/A	0.018	N/A	N/A	96	32	0.070
1	Stroubles Creek	5	0.014	0.015	0.327 (0.050)	1.12 (0.056)	90	33	0.041
2	Elliot Creek	15	0.017	0.018	0.492 (0.056)	1.17 (0.025)	19	19	0.0015
2	Elliot Creek	15	0.017	0.032	0.492 (0.056)	3.61 (0.076)	19	19	0.058
3	Elliot Creek	15	0.010	0.010	0.173 (0.057)	1 (0.018)	19	19	0.0018
3	Elliot Creek	15	0.010	0.025	0.173 (0.057)	5.99 (0.045)	19	19	0.041
3	Elliot Creek	15	0.010	0.027	0.173 (0.057)	7.28 (0.055)	19	19	0.048
4	N.F. Roanoke River	24	N/A	0.033	N/A	N/A	24	13	0.0029
5	N.F. Roanoke River	25	0.014	0.028	0.329 (0.058)	3.93 (0.033)	20	15	0.054
5	N.F. Roanoke River	25	0.014	0.025	0.329 (0.058)	3.33 (0.028)	20	20	0.015
6	Stroubles Creek	11	0.013	0.020	0.304 (0.056)	2.25 (0.041)	73	37	0.039
6	Stroubles Creek	11	0.013	0.030	0.304 (0.056)	4.91 (0.090)	73	19	0.058
7	Stroubles Creek	17	0.010	0.019	0.179 (0.057)	3.53 (0.024)	51	34	0.037
7	Stroubles Creek	17	0.010	0.031	0.179 (0.057)	8.94 (0.061)	51	27	0.076
8	Stroubles Creek	20	0.011	0.018	0.210 (0.057)	2.69 (0.019)	43	22	0.010
8	Stroubles Creek	20	0.011	0.028	0.210 (0.057)	6.43 (0.044)	43	17	0.063
9	Stroubles Creek	22	0.015	0.017	0.405 (0.057)	1.21 (0.014)	46	14	0.003
9	Stroubles Creek	22	0.015	0.031	0.405 (0.057)	3.98 (0.046)	46	18	0.012

Table 2.1: Raw data at each testing site for all entrainmemnt test trials

$\boldsymbol{p-value}$		
emb_0	$d_{50_{gravel}}$	u_*
0.143	0.027	0.002

Table 2.2: p-values associated with independent variables in relation to their effect on the measured erosive flux

2.5.3 Historic Model Performance and Adjustments

Since the most prevalent historic fine sediment entrainment models assume that the material is uniform in size and is being entrained from a bed also comprised of the same material, they do not account for the hiding effects provided from the larger grain sizes making up the stream bed. The models compared to the data collected from gravel streams where hiding effects are present are shown in figure 2.8.

Therefore, to produce accurate entrainment values, the models need to be updated to account for the hiding effects produced by the gravel beds if they are present. However, they also need to remain applicable for stream beds comprised of uniform fine sediment such as estuaries or coastal regions.

To accomplish this, both near-bed equilibrium SSC equations 2.9 and 2.5 of van Rijn (1984) and Smith and McLean (1977) will be altered by the hiding effect of the bed, or the

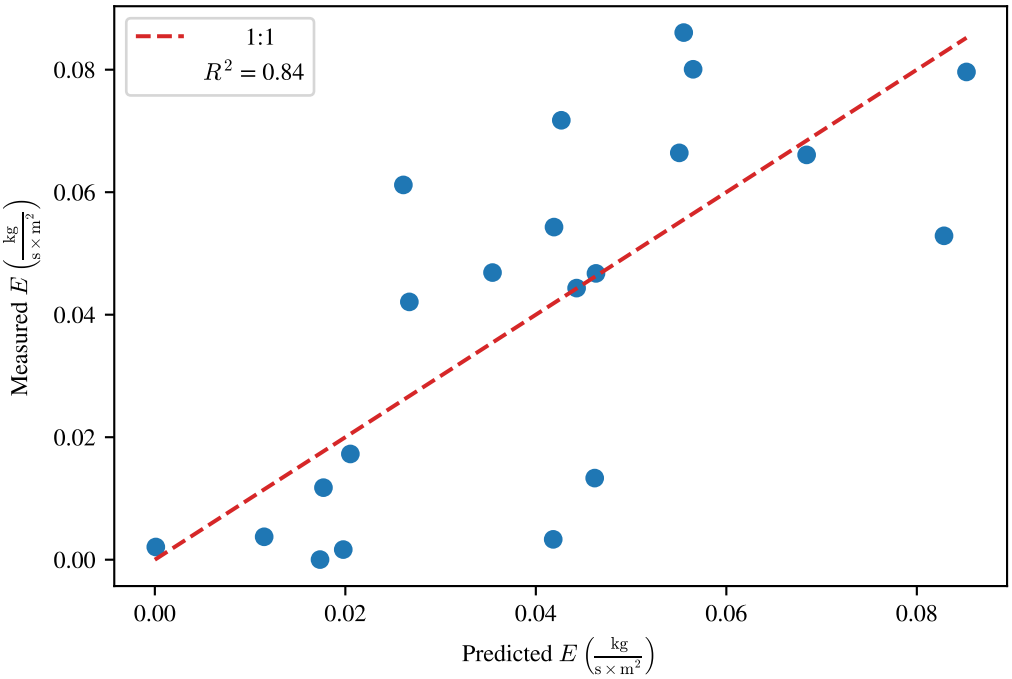

Figure 2.7: Measured versus predicted values of erosive fluxes after running a multiple linear regression with independent variables as emb_0, d_{50} of the gravel bed, and u_* applied to the bed

factor of the ratio of fines size to bed material size raised to some constant power, $-M$. Both of these models are dependent on the excess shear stress, T, that is applied to the bed material. For the test sites that had successful incipient conditions of fine sediment entrainment determined, the critical shear stress was able to be obtained, therefore, excess shear could be determined. Critical incipient shear velocities ranged from 0.010-0.017 m/s, or in terms of Shield's parameters, 0.15-0.44.

The updated models for van Rijn (1984) and Smith and McLean (1977) will therefore take the form of the following equations 2.25 and 2.26 respectively for the determination of entrainment coefficients.

$$E_s = 0.015 \frac{d_s}{b} \frac{T^{1.5}}{D_*} \left(\frac{d_{fines}}{d_{gravel}} \right)^{-M_1} \tag{2.25}$$

$$E_s = \frac{0.65 \gamma_0 T}{1 + \gamma_0 T} \left(\frac{d_{fines}}{d_{gravel}} \right)^{-M_2} \tag{2.26}$$

These can also be rearranged by moving the new term to the other side of the equations as follows and changing the sign of the constant M.

$$E_s \left(\frac{d_{fines}}{d_{gravel}} \right)^{M_1} = 0.015 \frac{d_s}{b} \frac{T^{1.5}}{D_*} \tag{2.27}$$

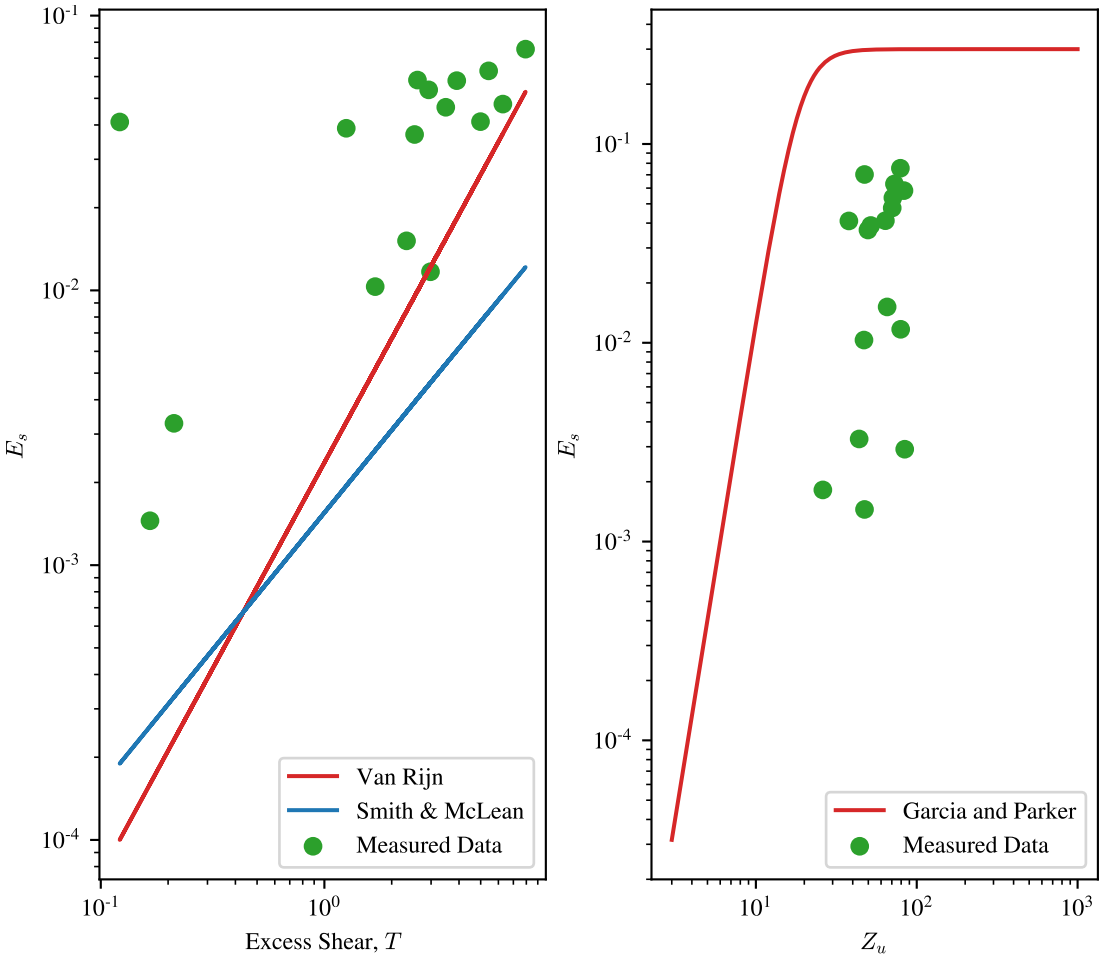

Figure 2.8: Models performance before any account of hiding effects assuming mud floc size as the determined $d_{f_{50}} = 133$ μm

$$E_s \left(\frac{d_{fines}}{d_{gravel}} \right)^{M_2} = \frac{0.65\gamma_0 T}{1 + \gamma_0 T} \tag{2.28}$$

This form is only used here as it allows for an easier view of model adjustment performance graphically.

When using the adjusted models portrayed in equations 2.27 and 2.28, the models produced the results displayed in figures 2.9 and 2.10. The constant M values that produced the best fit for the Van Rijn and Smith & McLean models were $M_1 = 0.123$ and $M_2 = 0.4$. These produced R^2 values of 0.73 and 0.80 respectively.

Similarly to the adjustment made to van Rijn (1984) and Smith and McLean (1977), the equation presented in Garcia and Parker (1991), equation 2.11, will be altered by a factor of fine sediment size to the size of the bed material hiding the sediment. Notice that the model equation for E_s is not altered in this case, but instead the equation for their input

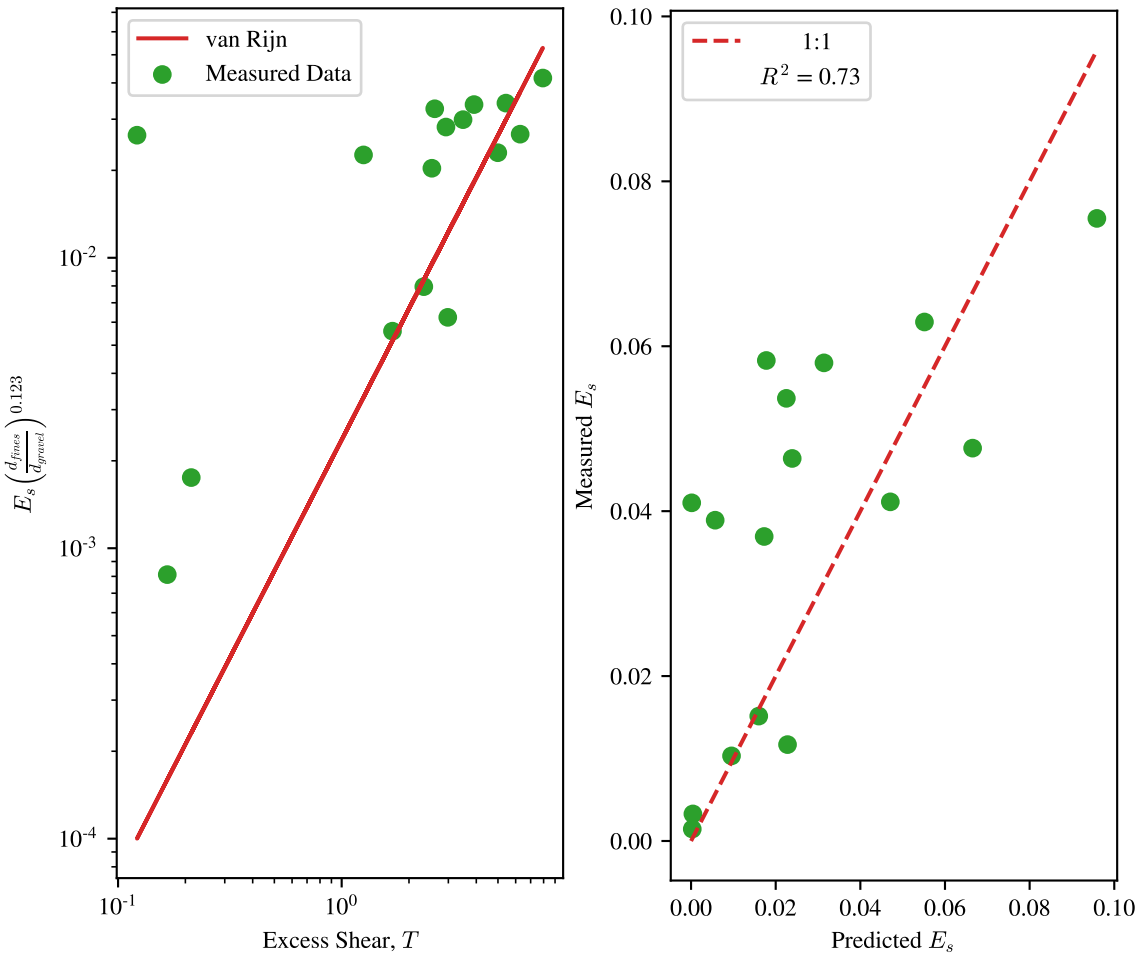

Figure 2.9: Comparison between the predicted and measured entrainment coefficients using the adjusted van Rijn (1984) model taking hiding effects of the gravel bed into account

parameter, Z_u, is adjusted by the hiding effect. This is seen as follows.

$$Z_u = \frac{u'_*}{\omega_s} R_p^n \left(\frac{d_{fines}}{d_{gravel}}\right)^{-M_3} \tag{2.29}$$

Where M is a constant. This will be the updated value that will be used in the original E_s model seen in equation 2.13. Leaving the Garcia and Parker (1991) equation for E_s the same and altering the equation for Z_u to equation 2.29 to account for the hiding effects of the bed produces the correction displayed in figure 2.11. In addition, the figure shows that even if the d_{50} was incorrectly assumed to be 133 μm, the adjusted model still produces good results. This is shown by assuming the d_{50} is equal to what we measured at the d_{16} and d_{84}. It can also be seen how the entrainment coefficient values change as the size of the fine material changes. This model adjustment provides the relation seen on the right in figure 2.11 with an $R^2 = 0.71$ for the adjusted prediction of entrainment for $d_{50} = 133\mu$m. A value

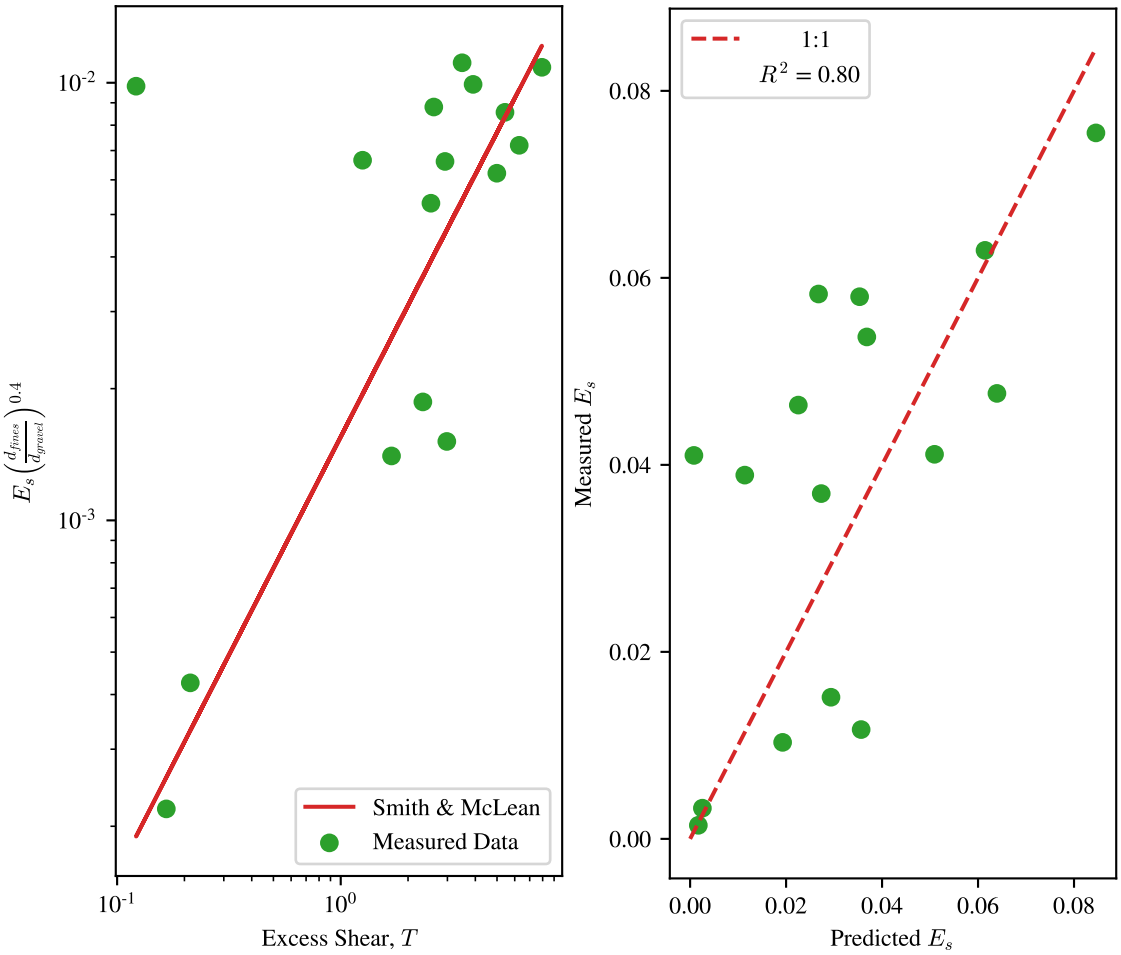

Figure 2.10: Comparison between the predicted and measured entrainment coefficients using the adjusted Smith and McLean (1977) model taking hiding effects of the gravel bed into account

of -0.362 provided the best fit for the constant M_3.

2.5.4 Terminal Point of Erosion

As stated previously, each trial with the Benthic Cannon was terminated once there was no more visible erosion of fine material occurring. It was at this point that the resulting embeddedness, or how far down into the surface layer the fines eroded to until the hiding effects of the surface layer were too strong. Knowing this value is important for quantifying the total mass being eroded or knowing how long erosion will occur under a given set of flow conditions. A new dimensionless parameter, S^*, was developed to predict the terminal erosion point, or the embeddedness level of the bed material. It is a function of the bed material size, the fine sediment size, the entrainment potential of the fines, the shear stress

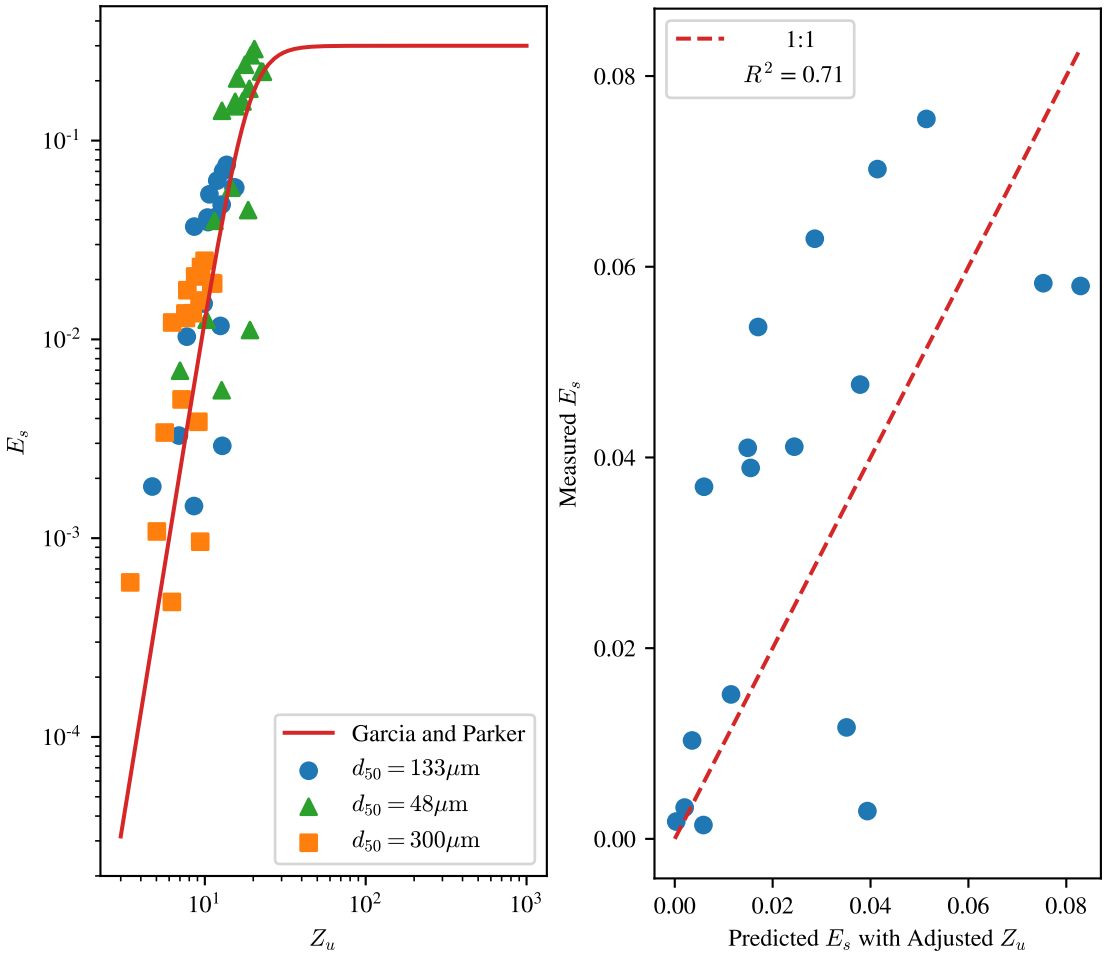

Figure 2.11: Garcia and Parker entrainment model after the adjustment to the equation for Z_u with different fine sediment sizes (left). The new measured versus predicted E_s values assuming $d_{50} = 133$ μm (right)

on the bed and the settling velocity of the fines.

$$emb_{final} = \frac{5337.4}{S^*} \tag{2.30}$$

$$S^* = \left(\frac{D_{*gravel}}{E_s}\right)^{0.38} + 5.5\left(\frac{u'_*}{\omega_s}\right) \tag{2.31}$$

$$D_* = d\left[\frac{R_s g}{v^2}\right]^{1/3} \tag{2.32}$$

D_* is a non dimensional grain size of the gravel surface layer bed material. The E_s value should be obtained using one of the adjusted models to account for hiding effects in the bed. The value obtained for emb_{final} is the percent embedded that the d_{50} of the gravel

bed will be left at given flow conditions. This will be referred to as the terminal point of erosion when no more entrainment of fine sediment will occur unless there is an increase in shear stress applied to the bed.

Using the new parameter, S^*, along with equation 2.30, the results portrayed in figure 2.12 were obtained. The model produced an R^2 value of 0.60 for $S^* \geq 53.374$. For $S^* < 53.374$, the embeddedness is assumed to stay at 100%. This could be a state where fines are just barely covering the surface layer of gravel or covering it by some thickness. Either way, the model should provide the finishing point of an erosional state of given conditions.

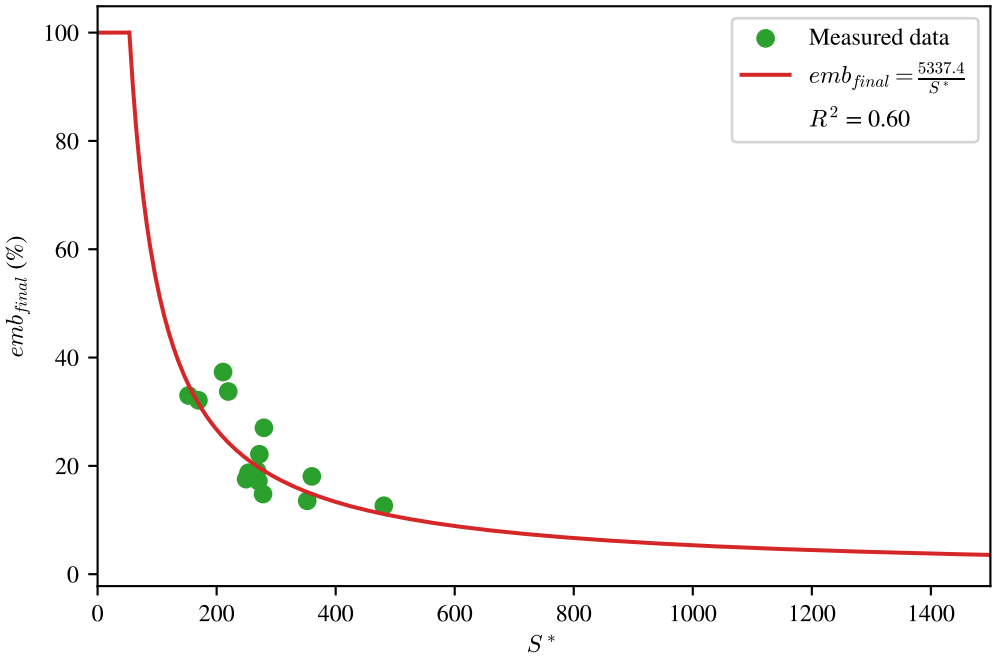

Figure 2.12: Prediction of the resulting embeddedness, emb_{final}, when the terminal point of erosion has been met using S^* predicting parameter

2.6 Discussion

2.6.1 Erosion Without Bed Mobilization

As discussed in section 2.5.1, all of the trials were conducted without the mobilization of the gravel surface layer. The largest shear stress applied during a trial was estimated to have had the ability to move gravel of maximum 3 mm in size. This stress was applied to a bed with gravel $d_{50} = 24$ mm. In addition, the site with the smallest d_{50} had a $d_{50} = 4.74$ mm. No gravel was observed to be mobilized through the Cannon. Even the smallest gravel patch remained unchanged through the testing. Because of this, it is safe to say that the muddy fine sediment was entrained without the mobilization of the bed. This goes against previous

assumptions that stated that entrainment and transport of fine sediment only will occur if the surface layer of gravel is disturbed (Harvey et al., 2012; Park and Hunt, 2018).

It is obvious that if the gravel surface layer were to be mobilized and its hiding effects eliminated, that the erosion of fines would be higher. However, with the rates experienced and the mass of fines that can be trapped in the pore space of the surface layer of gravel beds over a reach of stream bed area, it is crucial that we consider muddy fine sediment erosion without the surface layer being mobilized.

2.6.2 Parameter Effect on Erosion Rates

It was initially believed that the main parameters that would have would have a large effect on the rate of erosion at a given site would be the initial embeddedness, the d_{50} of the gravel surface layer, and the skin shear applied to the bed. Though all of these parameters did have an effect on the erosion rates measured, examining the p-values obtained from the multiple linear regression outlined in section 2.5.2, the initial embeddedness did not have a statistically significant effect on the rates of erosion. However, as both p-values for $d_{50_{gravel}}$ and the skin shear applied to the bed are less than 0.05, they do have a statistically significant effect on the rate of erosion from the bed into the water column.

However, knowing the initial embeddedness still provides valuable information. The initial embeddedness provides an idea of some volume or mass that is available within the top layer of gravel in a stream bed. It also provides a knowledge of available pore space for more muddy fine sediment to be deposited from the water column, but we did not recognize it having an effect on entrainment. For a future study, we believe that initial embeddedness could have a rising effect on entrainment with an increase in stream bed material size and decrease in embeddedness.

2.6.3 Altered Historic Models

With simple adjustments of three historic fine sediment entrainment models seen in equations 2.29, 2.25, and 2.26, the updated models were able to not only be applied to sediment sizes smaller than 62.5 μm, but all fine sediment in both gravel beds and beds comprised of the same material as the fine material being modeled in suspension.

Though the simple adjustment to the models all provide reasonable results and estimates for the entrainment coefficients measured in the field using the Benthic Cannon, the adjustment to the Smith and McLean model produced the best results with an $R^2 = 0.80$. However, this requires the determination of the excess shear stress being applied to the bed, so the critical Shield's parameter, τ^*_{cr}, needs to be determined. In the trials using the Benthic Cannon, this value was obtained by recognizing the incipient point at which fine sediment entered suspension. Estimating this value is possible based solely on the size of the sediment (Brownlie, 1981), but it essential to account for the hiding effects caused by the surface layer of gravel. This is as simple as multiplying the critical Shield's parameter by a factor of the ratio of grain size of the fines to the average grain size of the bed as discussed previously.

This is portrayed by (Einstein, 1950; Parker, 1990; Wilcock, 1993).

$$\xi_i = n\left(\frac{d_f}{d_{50_{bed}}}\right)^{-M} \tag{2.33}$$

Where M and n are constants. M is an exponent between 0 and 1.25. However, we believe that the initial embeddedness can be used here to alter the hiding effect for the determination of the critical or incipient Shield's number. The expression for the hiding effect would be altered to the following.

$$\xi_i = n\left(\frac{d_f}{(100 - emb_0)d_{50_{bed}}}\right)^{-M} \tag{2.34}$$

Though not enough incipient data was collected to draw conclusive results, utilizing Brownlie (1981) to estimate τ^*_{cr} and applying the hiding function provided in equation 2.34, an R^2 value of 0.88 was obtained for a measured versus predicted critical Shield's number (figure 2.13). $M = 0.23$ and $n = 1$ worked best for the prediction of the measured data. A future study of more incipient measurements could contribute to whether the assumption put forth in equation 2.34 is valid.

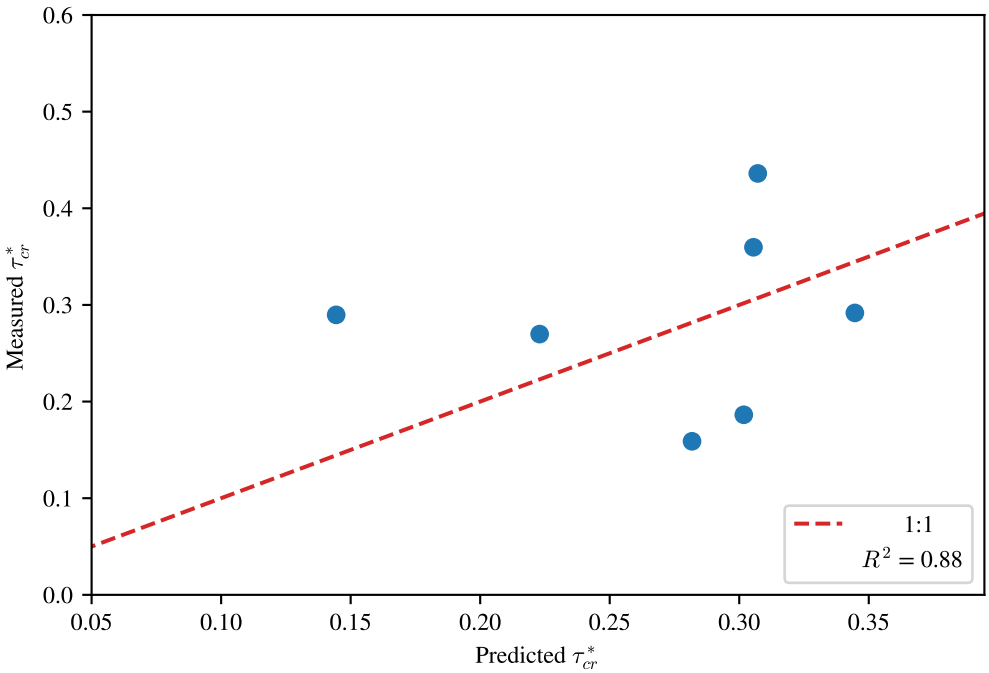

Figure 2.13: Prediction of critical shear stress accounting for hiding effects and utilizing the distance of not embedded material instead of the full d_{50} of the gravel as seen in equation 2.34

All three models produced reasonable results in estimating the entrainment coefficients. Garcia and Parker (1991) requires a settling velocity component while van Rijn (1984) and

Smith and McLean (1977) both require a critical shear stress value to determine the excess shear. Both the settling velocities and critical shear stresses can be determined from the size of the fine sediment in question. In addition, with the added term utilizing the ratio of fine sediment size to bed material size, both of those values are required regardless. So, no one model is easier than another to compute. Therefore, we suggest the utilization of the adjusted Smith and McLean (1977) model as it produces the best results with the measured data.

2.6.4 Terminal Point of Erosion

As seen in section 2.5.4, the dimensionless S^* parameter provides a relatively good estimate as to when the erosional shear forces and the hiding characteristics of the bed reach a point of equilibrium. This is helpful when trying to determine how much mass or volume of fines will be pulled from the pore space of the gravel bed.

If the initial embeddedness values are known, and the new model using S^* is utilized to determine the resulting embeddedness, the d_{50} of the bed can be used to estimate a void space volume of fines that will be eroded from the bed given a set of flow conditions.

$$V_{eroded} = d_{50_{gravel}} wL(emb_0 - emb_f)n \tag{2.35}$$

Using a porosity value, $n = V_v/V$, determined from the grain size distribution of the bed, and the change in embeddedness, the void space can be assumed to be filled completely with fine sediment. An estimate for the volume of fines eroded given flow conditions can be obtained over a reach length L given a bottom width w. This is a relatively simple way to estimate the mass or volume of fines eroded per area of stream bed.

2.7 Conclusions

From this study, it is shown that it is important that we explain the entrainment of fine muddy sediment from the stream bed into the water column even when the surface layer of gravel is not mobilized. Though past models perform well under the assumption that the bed material is of uniform size and is all comprised of the material being entrained into suspension, that is rarely the case in natural fluvial systems. It is shown that these models can be simply adjusted with a term similar to a hiding function utilizing the ratio of the size of the sediment in question of entrainment to the average size of the bed material. This was verified empirically using a new device named the Benthic Cannon which allows for *in situ* measurements of erosion rates of fine sediment. Measurements of how deep into the undisturbed gravel surface layer that fine sediment was entrained or unclogged from the bed aided in the creation of the new dimensionless parameter, S^*. This parameter helps predict the depth to which the given flow characteristics can overpower the hiding effects of the surface layer and unclog the fines from the pore space. This will be beneficial in quantifying the volume or mass of fines that will be brought into suspension given a storm event.

Chapter 3

Fine Sediment Deposition Within Mounded Gravel Nests

3.1 Introduction

Nocomis leptocephalus, hereafter referred to as Bluehead Chubs or "chubs", are a species of fish that construct mounded nests out of gravel that sit above the local stream bed to spawn. They are referred to as a "keystone" species because many other minnow species, referred to as "nest associates," also use chub-built nests to spawn (Vives, 1990). The chubs and nest associates can survive in multiple stream types and environments including degraded streams that may be polluted with high silt content (Johnston, 1994). They can survive even in degraded streams because the chubs provide a clean nest for all by first digging a small crater-shaped hole in the stream bed and then building the mound with cleaned pieces of gravel to a height that sits well above the ambient bed. The nest and its silt-free pore space therefore provide a spawning location that is both protected from predators yet still rich in oxygen (Maurakis et al., 1991).

The behavior of animals is often explained by acts of selfishness that provide a more beneficial outcome as a result of the selfish behavior. The selfish-herd theory states that individuals within a heard that occupy the center or most optimal position, have maximized the chance of survival (Hamilton, 1971). Though the original theory pertains to predation and therefore the benefit of being at the geometric center of the group, what it is pointing out is the benefit of being located in a zone of maximized fitness. Yet the zone of maximized fitness may not always be located at the geometric center of the group. This is especially true if stressors, such as abiotic factors, other than predation are at play.

Chubs have been observed to deposit their eggs on the upstream slope of the mounded nests they build (Maurakis et al., 1991). In addition, the chubs prevent other nest associates from spawning in the same pits as them showing that they specifically prioritize that spot for themselves. Because chubs prefer to spawn on the upstream side of the nest, rather than the geometric center of the nest, they may be responding to abiotic factors that are pushing them to see the front of the nest as the one that provides the greatest fitness benefit for the survival of their offspring.

It has been suggested that deposition of fine sediment, or siltation, on or within the nest may be a factor chubs are considering when choosing a location in the nest to spawn (Peoples et al., 2011). Wallin (1992) observed that fine sediment deposits on the downstream surface of the nest begin to be visually evident approximately two days after the nest has

been built. The presence of fine sediment over the back of the nest and the chub's preference to spawn in the front of the nest has led to the idea that chubs actively avoid locations in the nest that tend to experience siltation with time. This fits the notion that chubs avoid locations that might present unfavorable abiotic conditions for their eggs since the presence of silt is known to lead, in general, to decreased levels of oxygen in pore-space water due to inhibited flow and active oxygen consumption due to microbial respiration in the fine sediment (Collins et al., 2017; Sear et al., 2017). Siltation on the upstream side of the nest is not commonly observed because the current of the streams and the fanning of all of the fish activity over the upstream half of the nest aids in keeping the gravel clean of silt (Potts et al., 1988; Wallin, 1992). This includes the chubs moving the gravel around where their eggs are spawned to keep the area clean of silt while the fertilized eggs are present.

Silt can arrive at the nest through different pathways due to the nature of the hydraulics around and through the nest. Nests sit above the surrounding surface of the stream bed. As a result, the local flow field surrounding the nest is altered relative to that of the ambient flow. Flows accelerate over and around the front of the nest due to contraction effects (Henderson, 1966). On the downstream side of the nest, flow decelerates and may even separate to form a protected low-velocity or even recirculation region (Mendoza and Shen, 1990; Strom and Papanicolaou, 2007; Papanicolaou et al., 2012). The sheltered, low-pressure region of a wake created by the nest, or any rock or bedform in the river, and secondary flow cells provide conditions favorable for the deposition and build-up of fine sediment being carried over or around the obstacle with the bulk fluid (Kostaschuk et al., 2009; Papanicolaou et al., 2012). The observation that siltation is observed on the downstream or wake side surface of the nest with time is congruent with the concept of sedimentation in the protected wake zone of an obstacle.

Fine particles can also arrive in plane gravel beds or raised bedforms (similar to nests), through turbulent diffusion and settling (Krishnappan and Engel, 2006; Mooneyham and Strom, 2018b). This is true even in cases when flow conditions should prevent the settling of fine sediment, i.e., cases when the turbulent shear velocity is much greater than the settling velocity of the sediment (suspension thresholds are typically set when the two are nearly equal (García, 2008; Lamb and Venditti, 2016)). The primary reason for this is that sediment that settles or is turbulently advected near the bed can become trapped in the low-velocity pore space of the bed. Mooneyham and Strom (2018b) found that the ability of a bed to capture fine sediment increases with pore space. So one might expect that the clean gravel nest would have ample pore space and the ability to capture fine sediment.

Another mechanism of fine sediment transport to the nest could be that of advective hyporheic pumping. The changes in velocity and depth brought on by the presence of the raised nests will lead to time-averaged variation in pressure along the surface of the bed and nest that may drive surface water through the nest similar to what is observed in sand dunes (Elliott and Brooks, 1997; Janssen et al., 2012; Hester et al., 2013). If this occurs, then there is a chance that sediment advected into the pore space along with the surface water may settle or be filtered out if the suspended sediment sizes are of the same order as the pore space similar to what has been observed in sand dunes and ripples (Packman et al., 2000;

Dallmann et al., 2020).

3.2 Research Questions and Study Goals

Though siltation has not been studied in chub nests, deposits of fine sediment in the wake region of the nest have been visually observed. Furthermore, it is known that fine sediment can deposit within plane gravel beds with no extrusion of the bed in the form of a nest to create a larger protected wake zone. For example, Mooneyham and Strom (2018b) showed that clay-sized particles deposited within plane gravel beds even under high bed shear stresses and that deposition of the clay increased with more available pore space. Furthermore, fine sediment is known to be filtered out of hyporheic flow passing through raised sand dunes (e.g., Packman et al., 2000). We, therefore, expect that fine clay and silt-sized mud can deposit within chub nests either through surface sedimentation due to the low-velocity wake structure, sedimentation due to settling in the low-velocity pore space, or through settling of sediment carried with the surface water that is being hyporheically advected through the nest.

The broader work associated with this study aims to determine if chubs are accounting for siltation patterns when deciding where to spawn on the nest. As a first step toward that end, we here aim to measure the siltation pattern within synthetic mounded gravel nests placed in a stream known to be an active spawning reach for chubs. The intermediate questions we seek to answer with data from the study are: (1) is siltation within the nest larger in the front or back of the nest, (2) is the siltation coming from ambient surface sedimentation or settling of hyporheically-advected suspended material within the pore space, (3) how do factors such as nest position within the river (thalweg vs bank) or nest physical geometry impact siltation rates within the nest given ambient river conditions?

We explore these three research questions by deploying artificial chub nests in the same habitat they use for reproduction during non-spawning seasons to assess the influence of fine sediment deposition within the nests without the presence of fish.

3.3 Methods

3.3.1 Overview

The mass of fine sediment that accumulates within different locations in a bluehead chub nest was determined by deploying artificial nests in a local creek between chub spawning seasons. The artificial nests were constructed with gravel collected from chub-built nests at the end of the previous spawning season. Sediment traps were installed in each nest to determine the spatial sedimentation pattern. Nests were deployed in the thelweg and near the bank for a range of flow conditions and the mass of sediment captured in each sampler during each deployment time was measured. Ambient conditions in the river were measured with a stage and turbidity meter to estimate the capture efficiency of a given nest; the

efficiency is a ratio of the captured mass to the estimated total mass delivered to the nest by advection.

3.3.2 Nest and Sampler Deployment and Retrieval

Enough gravel was collected after the spawning season to allow for two nests to be deployed at a given time. The gravel from the nest had d_{16}, d_{50}, and d_{84} of 10, 15, and 23 mm. Porosity, as determined by Fuller (2022) of 0.4. Before the artificial nests were constructed and deployed in the field, the gravel was washed to ensure all fine sediment captured during the study was deposited in the nest from suspended sediment in the stream during the deployment. Seven sediment-collecting jars were placed in each nest. Each jar had a 7.62 cm diameter opening, was 5 cm deep, and was filled with the same gravel used to construct the nest. The jars are placed within the nest in the orientation displayed in figure 3.1 with the opening of the jars facing up vertically.

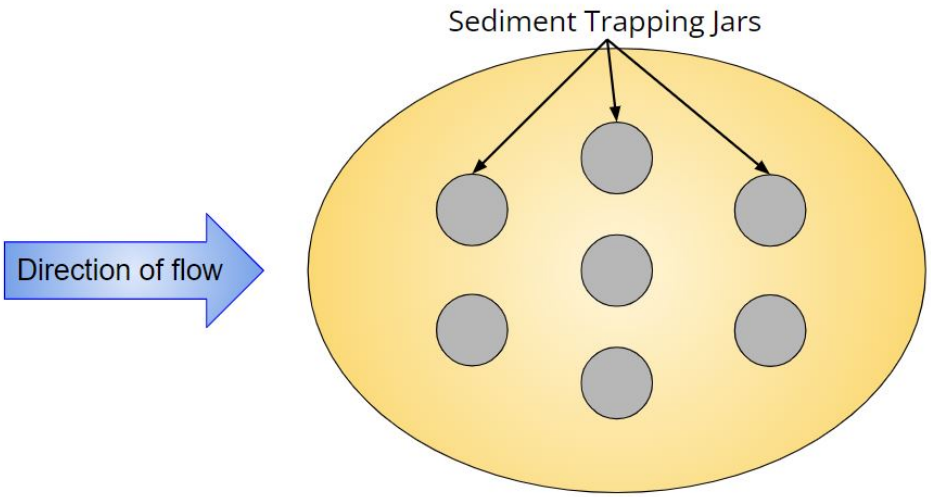

Figure 3.1: Orientation of sediment capturing jars spatially distributed throughout nest from a plan view

Chub-selected gravel for the nests was limited and needed to be reused for each deployment of two nests. Nest stones were therefore placed on a patch of porous fabric to enhance recovery of the nest stones after each deployment. For the actual construction, the fabric was first anchored to the streambed. The sedimentation jar samplers were then arranged on the fabric starting with the most upstream sampler and then working downstream to ensure that any suspended sediment generated by operator movement in the stream was not collected before placement of the nest stones. Once the jars were in place, the nest was formed by placing the gravel in an ellipsoid mound with the long axis of the nest in the downstream direction. The length, or long axis in the downstream direction (l), width, or

short axis in the lateral direction (w), and height (h) of each nest were then measured. The height of the nest was determined by measuring the water depth on each side of the nest (from water surface to stream bed), taking the average of those two values, and subtracting the water depth measured from the water surface to the middle of the nest, or the highest point. One nest was placed in the thalweg of the cross-section where the water velocities visually appeared to be the fastest. The other was placed closer to the bank where velocities visually appeared to be slower than that of the thalweg (Figure 3.2).

Figure 3.2: Nests deployed in the stream and the anchored logger recording stage and turbidity.

An RBR duo3 data logger with an attached optical backscatter sensor (OBS) and pressure transducer (Figure 3.2) was deployed just upstream of the nests and was set to measure turbidity (in NTUs) and depth at a rate of 0.1 Hz.

The nests were left in the stream for different lengths of time, ranging from 2 to 6 days depending on flow and weather conditions. It was crucial that the nest gravel was not lost in the case of a high flow event. Therefore, if larger storms were expected, the nests were collected, and the deployment was terminated. In addition, during testing, it was determined that the collection jars became filled with fine sediment after 5 to 6 days of baseflow conditions.

The collection jars are retrieved in the reverse order that they were placed to ensure that sediment stirred up by the retrieval process was not sampled by a downstream jar. To extract the jars, the top of the nest gravel was carefully brushed away to expose a jar and allow for the lid to be installed. Once the lid was installed the jar was removed from the nest. This process was repeated until all jars were collected. Following extraction fo the sampling jars, all of the nest gravel was captured and retrieved by picking up the porous fabric. The fabric and nest gravel were cleaned for reuse between deployments.

3.3.3 Post-Deployment Sample Processing

The content of each sampling jar was wet sieved to determine the mass of fine sediment that had deposited into the nest. Everything was passed through the 6.35 mm sieve to remove the nest gravel to be reused that filled the sediment jars. The fine sediment in each jar that passed the sieve was then further split with the 230 sieve (mesh opening of 62.5 μm) into sand ($d > 62.5$ μm) and mud ($d < 62.5$ μm).

The sand samples for each jar were immediately transferred to the oven to remove any moisture by drying overnight. The dry mass of sand accumulated in each jar was measured by weighing after drying. The water and mud mixture ($d < 62.5$ μm) produced by wet sieving was put into a tall graduated cylinder, and left for multiple days to allow the mud to settle to the bottom of the cylinder. The clear water was then carefully decanted until only a thick mud slurry remained at the bottom of the cylinder. The slurry was placed in a pre-weighed aluminum container and dried in the oven. The dried sample and container were then weighed to obtain the dry mass of the mud. An example of sediment captured and the wet samples separated by sand and mud is shown in figure 3.3.

Figure 3.3: (a) Fine sediment accumulated in the sediment capturing jars. (b) Separated samples from the jars by sediment greater than 62.5 μm and less than 62.5 μm

Processing of the sediment collected in the jars provided the total mass of sand and the total mass of mud collected over a known number of days for each jar. Since each jar was placed in a particular location in the nest, the raw mass data from the samples provided the means of measuring the spatial siltation pattern within the nest. More specifically, it is important to determine if more sediment is being trapped in the upstream or downstream side of the nest. For this analysis, the three jars across the middle of the nest were neglected and the mass accumulated in the remaining four jars was summed (Figure 3.1). The two upstream and two downstream jars were summed separately and the ratio of mass captured in the upstream versus downstream jars were compared.

3.3.4 Mass Capture Efficiency

Larger quantities of suspended sediment in the creek will likely lead to larger amounts of sediment being captured in the sampler. Furthermore, leaving the sampler out for longer in

the creek will also lead to large quantities of fine sediment being captured in the sampler all else being equal. Therefore, to help normalize the results we present both the total mass of the sand and mud fraction as well as and mass capture efficiency of the nest as a whole.

The capture efficiency (r_c) of the nests is defined as the ratio,

$$r_c = \frac{M_c}{M_p} \tag{3.1}$$

where M_c is the mass of sediment captured by the nest and M_p is the mass of sediment estimated to pass through the nest. As stated previously, seven sediment-capturing jars were placed within each nest. These were used to estimate M_c for each nest as follows:

$$M_c = \frac{M_t}{7A_j} A_n \tag{3.2}$$

In equation 3.2, M_t is the total mass captured in the jars, A_j is the area of the opening of one jar, and A_n is the area of the nest. Because the nests were arranged in an ellipsoid shape, the area of the nest was computed as

$$A_n = \pi \left(\frac{lw}{4} \right) \tag{3.3}$$

Therefore, estimating the capture efficiency of the nest was based on M_c estimated from the jar samples, the geometry of the nest, and the estimated M_p value.

M_p was estimated using a concentration of sediment in the ambient stream water outside of the nest, C, the estimated pore-water velocity, the nest frontal inflow area, the porosity of the nest, and the time for which the samplers were deployed.

Time series of the pore water velocity flowing through the nest and the suspended sediment concentration of the water entering the nest were driven by the data gathered outside of the nest with the RBR OBS and pressure transducer. The OBS measures the turbidity of the water in NTUs. These values were correlated to suspended sediment concentrations using known masses of fine sediment collected from Toms Creek added to a known volume of water in a mixing tank. These values produced the relationship, $C = 0.002(NTU) - 0.0065$ ($R^2 = 1$) where C is in kg/m^3.

The velocity of water passing through the nest was estimated with the RBR depth measurements, measurements of the ambient approach velocity, and 3D permeable-bed hydrodynamic simulations of flow through the nest (Yang et al., 2024). To do this, the velocity and water depth or stage were first measured at each nest deployment location during both low and high-flow events. With this data, the lower and upper bounds on the ambient approach velocity, U_a, in the stream during the times of deployment were estimated to be 0.1 and 1 m/s. The lower and upper bounds on the approach velocity were then used as the approach velocity in the 3D permeable-bed computational fluid dynamics (CFD) simulations of the mounded chub nest carried out by Virginia Tech collaborators Ph.D. student Huan Yang and Dr. Hosein Foroutan. Huan Yang then provided average longitudinal pore-water

velocity values through the nest from the CFD simulations, and these values were integrated into a single average pore-water velocity, U_p, for the nest. For example, the U_p values associated with the ambient stream velocities of 0.1 and 1 m/s were $U_p = 0.012$ and 0.169 m/s, respectively. These values were used to linearly interpolate a pore velocity corresponding with any ambient stream velocity, which was estimated by the stage being recorded.

The RBR data therefore provides time series estimates of C and U_p at a resolution of 0.1 Hz during each deployment. Taking the product of these time series results in a maximum mass flux time series passing through the nest. When integrated over the frontal pore space area of the nest, or multiplying by nA_f, where n is the porosity, if C and U_p are assumed to be area-averaged values, a mass flow rate time series can be obtained.

$$\dot{M}(t) = U_p C(t) n A_f \tag{3.4}$$

where A_f is assumed to be half of an ellipse,

$$A_f = \frac{\pi}{2}\left(\frac{hw}{4}\right) \tag{3.5}$$

Integrating $\dot{M}$ over time provides M_p. This is demonstrated in the following relationships.

$$M_p = \int_{t_0}^{t_f} \dot{M}(t) dt \tag{3.6}$$

with t_0 being the time at which the nest deployment begins and t_f being equal to the time when the mass capture samples were collected.

3.4 Results

3.4.1 Spatial Siltation Comparison

After combining the mass accumulated in the sampling jars placed toward the upstream and downstream part of the nest and separating them into mud and sand components (greater than or less than 62.5 μm), the ratio that deposited in the front half versus the back half of the nest was determined. The results are shown in figure 3.4.

It is seen that in all 10 nests examined, mud was preferentially deposited in the upstream half of the nest. That is, more mud deposited in the front than the back of the nest. The sand size sediment did not have a consistent spatial trend. In fact, 5 of the 10 nests had more sand depositing in the front while 5 had more sand depositing in the back. There was also no consistent trend in the ratio of mud sized to sand sized sediment depositing within the nests. The ratio of mud mass to sand mass captured per nest ranged from 0.26-2.43.

3.4.2 Nest Dimensions Effect on Capture Efficiency

The data collected from each nest was compiled to determine the effect of the nest dimensions on how efficient the nests were in capturing the sediment flowing through it. Capture

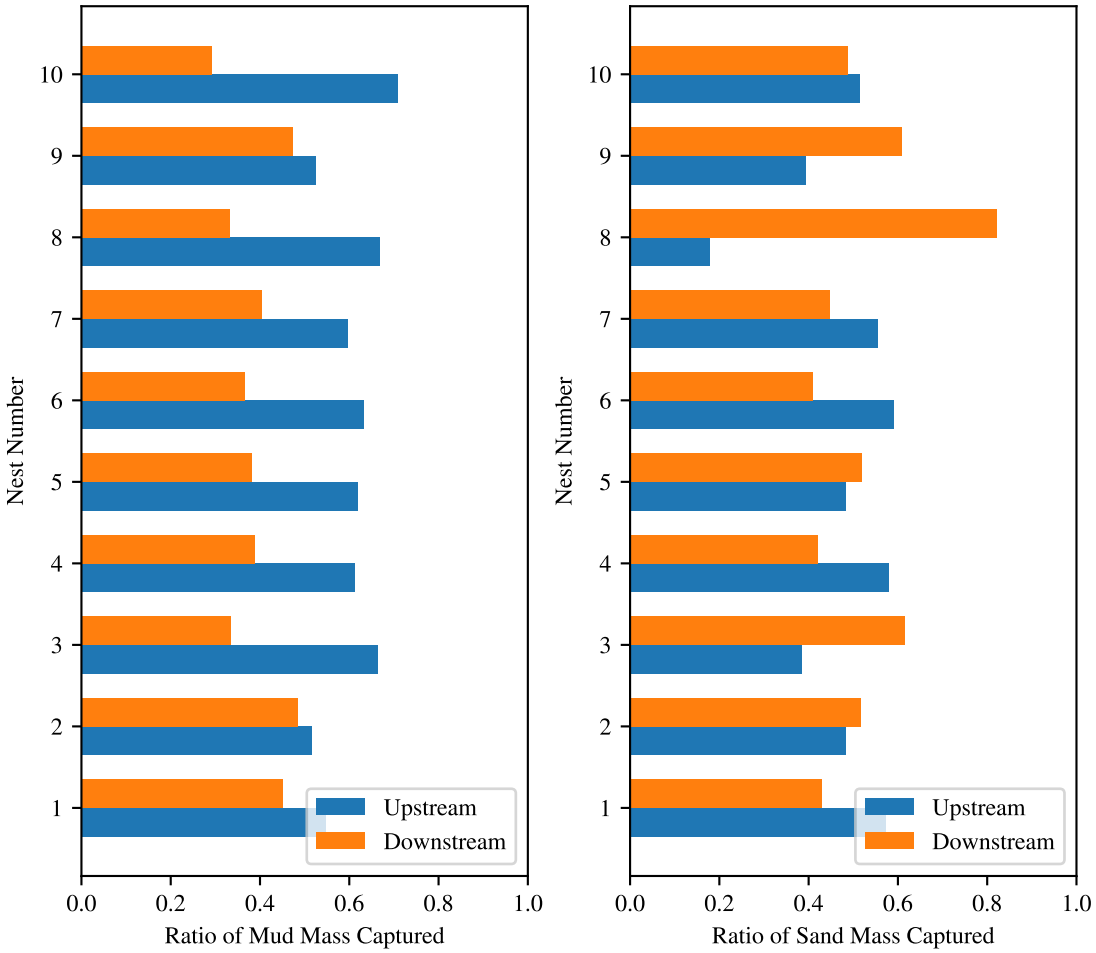

Figure 3.4: Mud and sand mass ratio distributions between the upstream and downstream halves of the nests

efficiencies measured ranged between 0.002 and 0.185. The length, width, and height of the nests were all separately compared to the capture efficiency calculated (figure 3.5). The length and height of the nests had the largest effect with R^2 values equal to 0.76 and 0.54 respectively. The width showed the least effect on capture efficiency with $R^2 = 0.24$.

3.5 Discussion

3.5.1 Spatial Siltation Comparison

As seen in figure 3.4, the sediment classified as mud, or anything $d < 62.5$ μm, primarily deposited in the upstream half of the nest in every single nest that was deployed. The sand class, anything captured with $d > 62.5$ μm, however, was more random in which half of the nest captured more. Exactly half of the nests experienced more deposition of the sand class

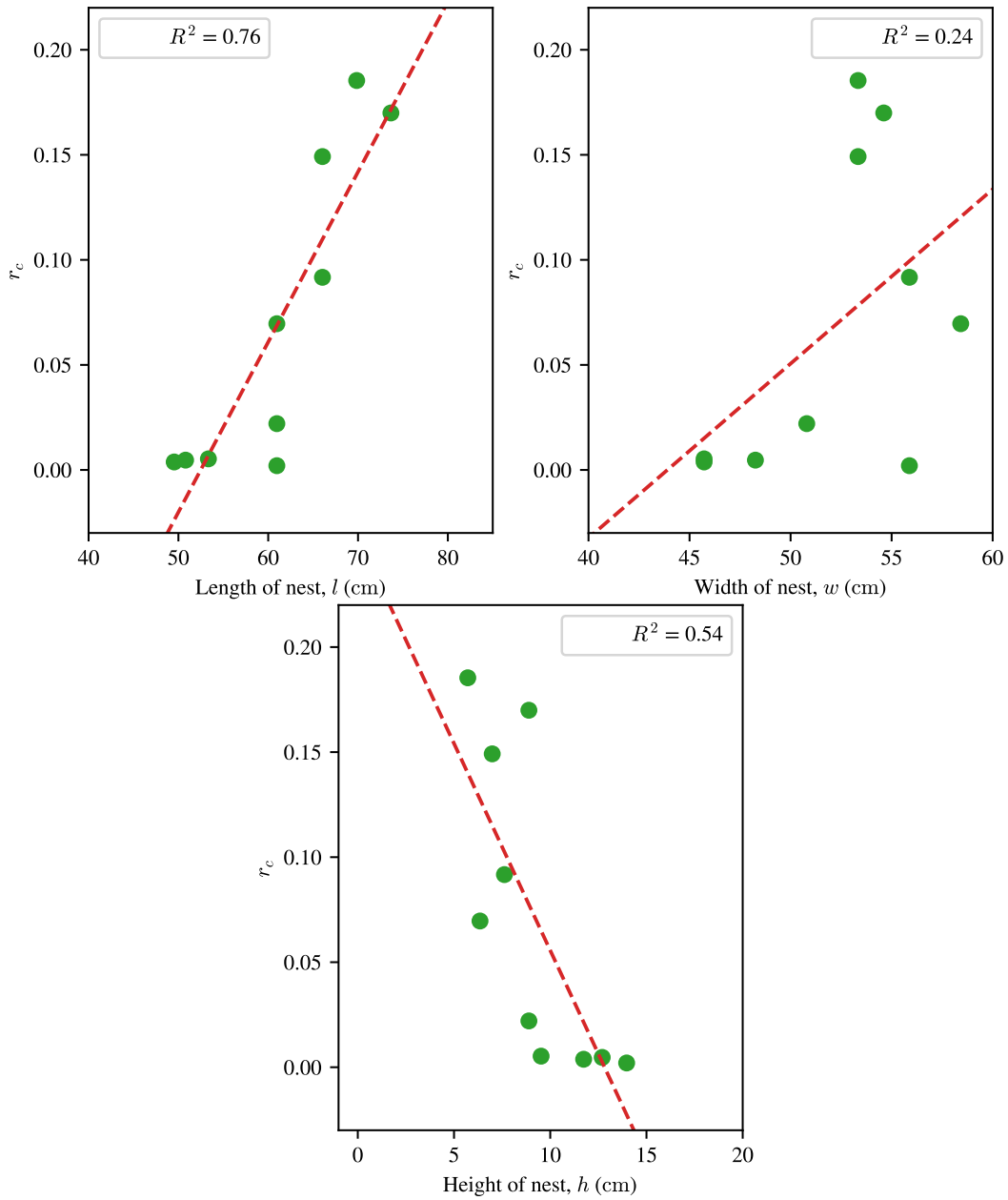

Figure 3.5: Length, width, and height of the nests compared to the capture efficiency for each nest

in the upstream of the nest, and the rest had more in the downstream by mass.

Each of the three possible pathways for mud to make its way into the nest outlined in the introduction can be linked to a hypothetical deposition pattern. Suppose the material found in the nest is primarily arriving by surface deposition due to the presence of the low-velocity wake. In that case, it is reasonable to expect that the accumulation amounts would be higher in the back of the nest (Figure 3.6). Suppose it was due to sediment arriving at the bed

from generic turbulent diffusion or settling. In that case, one might expect no strong spatial preference in the accumulated mass. If the arrival pathway is hyporheic pumping through the nest (Figure 3.6), and the settling velocity of the mud is high enough or the pore water velocity is slow enough, then one would expect higher deposition amounts in the front of the nest. The reason for this is that the steady-state solution to the suspended sediment transport equation, which would provide a solution for $C = C(x)$ is an exponential function that decays with distance through the nest, x (Culp et al., 2021). Because deposition scales with the local concentration and settling velocity of the sediment, one would expect higher volumes of sediment to deposition at the front of the nest.

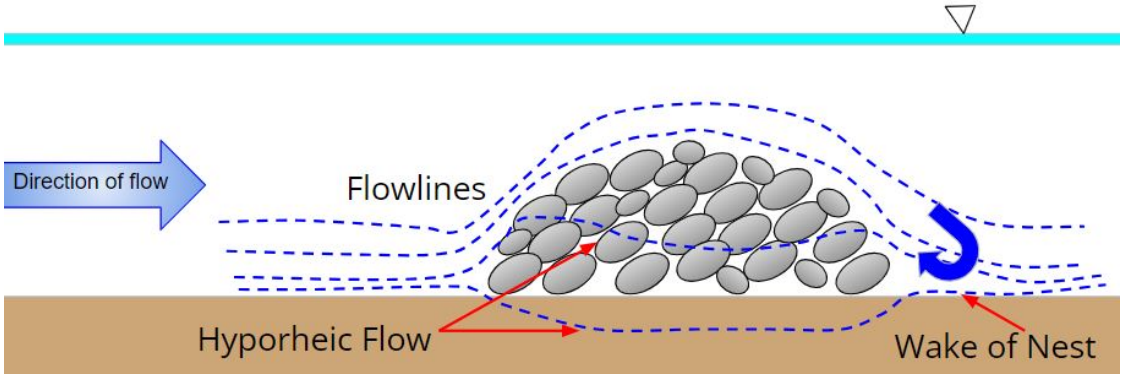

Figure 3.6: Flow around a chub nest

Though the exact pathway the fine sediment took from the stream to the sampling jars is unknown, we are led to believe that the sediment size less than 62.5 μm deposited while traveling through the low-velocity pore space of the nest as hyporheic flow. As it made its way through the nest in suspension at some concentration, we believe that the water/sediment mixture gets stripped of the sediment, thus filtering out and decreasing C as the mixture moves through the nest.

This idea is contrary to the previous belief that fine sediment will accumulate more heavily on the downstream side of the nest due to the wake or separation eddy caused by the nest allowing for the sediment to "rain down" and get caught in the re-circulation of the water to deposit. The deposition on the downstream side of the nest still occurs, but the reason the upstream side appears "clean" is believed to be due to the cleaning activity of the chubs while embryos are present (Wallin, 1992).

The deposited mass of sediment greater in size than 62.5 μm showed no consistent spatial trend within the nest. One might have expected the coarser sand fraction to follow the spatial distribution of the mud if the primary transport pathway into the nest was hyporheic pumping. However, our data does not show this same pattern. A potential reason for the lack of spatial pattern might be that the majority of the sand that entered the nest settled to a level below the top of the jars before reaching the first sampling jar (Figure 3.1).

The advective length scale of a particle in the x or along the current direction, L_a, is:

$$L_a = \frac{U_p h_s}{w_s} \tag{3.7}$$

where h_s is the vertical height over which the particle must settle and w_s is the settling velocity of the particle. Therefore, as w_s increases moving from mud to sand, L_a will decrease.

Though our qualitative pattern analysis is not capable of precisely defining the pathway the sediment took to its deposition location, measurements of captured mass within the nest are inconsistent with the visual observations made of the surface of the nest; where larger amounts of silt have been observed on the downstream side. This does suggest that siltation within the nest is likely not primarily driven by surface sedimentation. While the data does support the idea that sediment is primarily arriving via hyporehic flow, it is important to recognize that the nests being used for experimentation were not actively being used by chubs or nest associates during the deployment. Therefore, the fish were not cleaning off the front of the nests or interacting with them in any way. Visually, an equal amount of surface deposition was distributed over the entire nest.

3.5.2 Nest Dimensions and Capture Efficiency

The largest correlations between sediment capture efficiency and the nest geometry parameters existed between the length and height of the nest and the corresponding capture efficiencies. It is important to note that a large part of the correlations is due to how the capture efficiency of a nest is determined. This is because the frontal area and total area of the nest are used to determine the mass that passed through the nest and the mass captured by the nest respectively. The height of the nest is used to calculate the frontal area and the length to calculate the total area. The width is used in the determination of both areas. This is why the width does not have as strong of a correlation because it gets canceled out when calculating the capture efficiency.

Due to how the capture efficiency is calculated, the height and length of the nest should have an inverse but equal effect on the capture efficiency of the nest, but it is seen that the length has a greater effect on r_c. This makes sense and supports our hypothesis that as the length of the nest in the downstream direction increases, the amount captured should increase since there is a longer distance and area in which the sediment is being stripped, or filtered, from the water column.

The height of the nests had an inverse relationship with the capture efficiencies produced. This makes sense again based on the calculation of r_c. However, this can also be due to the physical arrangement of the nest and jars. Roughly the same volume of sediment was used to create each nest. So if a nest is taller, then it is likely that the nest is also shorter in length. Therefore, taller nests are thought to be less efficient silt traps if they are also shorter in length. Another potential reason that a taller nest might be less efficient is that it might be easier for the sediment moving through the nest higher up to bypass the samplers due to the increased height over which the sediment must settle. If h_s goes up,

then L_a increases (equation 3.7) and potentially exceeds the length of the path through the nest. Thereby bypassing capture in the jars.

Additionally, in the case of "rain down" deposition, the jars most likely miss more and more of the material "raining down" on the nest as the height of the nest increases due to some of it being trapped on layers of gravel above the jars. If the sediment was primarily entering the nest along this pathway, then taller nests would do a better job at protecting the eggs buried lower from being suffocation by fine sediment as more sediment would be getting trapped on higher layers of gravel getting filtered before reaching the bottom of the nest.

3.6 Conclusions

Bluehead chubs spawn their eggs in mounded nests that they create by picking up pieces of gravel with their mouth and placing them in a mounded pile. The Chubs consistently place their eggs in the upstream half of the nest. Fine sediment poses a risk to the Chubs' eggs as it can clog the pore space between the gravel, potentially block dissolved oxygen from getting to the eggs, and may even add an oxygen demand to the nest.

Though it has been suggested that the chubs place their eggs in the upstream portion of the nest because more fine sediment deposits in the back of the nest, our study shows that more fine muddy sediment deposits in the upstream side of the nest relative to the downstream. This leads us to believe that the siltation in the nest primarily occurs as sediment gets stripped from the water being advected through the nest pore space. We expect that the visual disparity in the amount of silt on the surface of the nest in the field during spawning season (i.e., larger quantities of silt on the surface of the downstream side of the nest relative to the upstream side), is due to a combination of the low-speed wake zone flow field and the active cleaning of the upstream portion of the nest by fish. Without the presence of the fish and their active cleaning of the front, the sedimentation data from these experiments suggest that the surface pattern evident during spawning does not fit the spatial pattern of material deposited in the nest. It is unknown if the internal deposition pattern would change if fish were actively fanning the front of the nest to keep the surface clear of fines.

Data from this study suggest that nests with a more elongated alignment with the downstream flow direction will have a higher sediment trapping efficiency relative to nests that have their elongated axis perpendicular to the flow. Additionally, shorter nests appear to have higher trapping efficiencies than taller nests. Taken together, nests that are taller in height and shorter in the direction aligned with the current will have the lowest trapping efficiencies. This means that nests that are taller and shorter in the downstream direction will accumulate less fine sediment than a nest that is shorter in height and longer in length.

Chapter 4

Conclusions

Fine muddy sediment (grain size < 0.1 mm), comprised of both organic and inorganic matter, is a natural product found throughout the entire fluvial system including the floodplains, suspended in the water column, and deposited in the stream beds. Due to the small size, the fine sediment primarily travels through the system as a suspended load. In the past has been treated as a washload where it has been assumed to never deposit until reaching a near-zero velocity region. However, due to the amount of muddy fine material found within stream beds, it is important to shift from this oversimplification and treat fine sediment transport through the system as a series of depositional and erosive events. The presence of fine sediment in fluvial systems has a multitude of effects on humans, the aquatic ecosystem, and land building. Though beneficial for areas where land loss is of concern, most effects adversely impact the fluvial environment and those that depend on it, both human and aquatic biota. Anthropogenic changes to the earth are also increasing the supply of fine sediment to fluvial systems. For these reasons, we believe it to be crucial to transition the strategy of fine sediment transport modeling to multiple series of depositional and erosive events through the system.

While it is accepted that mud deposits and is stored in the bed until resuspension occurs, the lack of understanding of entrainment fluxes of mud from the stream bed contributes to fine muddy sediment being ignored in transport models. Chapter 2 aimed to study the entrainment of mud from immobile gravel stream beds. The key findings are summarized as follows.

1. The assumption that the fine sediment stored in a stream bed will only resuspend once the bed material is mobilized is invalid as entrainment was seen in all cases with the gravel bed material remaining immobile. Therefore, we believe that muddy sediment is being entrained and depositing more frequently than what was assumed before, during storm events that do not reach bankfull conditions, or conditions to mobilize the gravel surface layer.

2. Entrainment of loose muddy sediment stored in the stream bed can be modeled using the framework of classic sand entrainment models adjusted to account for the hiding effects that the gravel bed provides for the fine sediment.

3. Embeddedness did not prove a statistically significant effect on the entrainment fluxes measured, but we believe that as gravel grain size increases, it will have a greater effect on the critical shear value for entrainment

4. The terminal point of entrainment, reported as a final embeddedness, can be predicted given stream bed and flow characteristics.

Chapter 3 examined depositional tendencies of fine sediment as it pertains to fish species that are directly affected by its presence in the streams. Data was collected using artificial Bluehead Chub spawning nests to provide a better understanding to their typical spawning behavior of placing their eggs in the upstream side of their nests. The findings are summarized as follows.

1. For sediment $d < 62.5$ μm, more deposition was consistently seen in the upstream half of the nest, where sediment $d > 62.5$ μm showed inconsistent depositional patterns throughout the gravel nests. We believe that the clean upstream faces of real chub nests observed in the field is due to the chubs' consistent cleaning of the upstream gravel while nests are active.

2. Mud is believed to deposit primarily in the nest by getting stripped from the water/sediment mixture being hyporheically pumped through the nest.

3. No consistent depositional patterns were seen between the thalweg and bank nests.

4. As nest shape got longer in the downstream direction, the capture efficiency of the nest increased. As height of the nest increased, the capture efficiency decreased. However, we believe that the effect of the height was due to the sampling jars sitting on the bottom of the nest and fines got trapped on upper layers of gravel within the nest.

In the future, it would be helpful to further investigate the effects of embeddedness or a volume of fines stored or volume available for storage on the entrainment and deposition of fine sediment within plane gravel beds. More data on critical Shield's parameters should be collected with a larger range of gravel grain sizes and a range of embeddedness values. A wider test section than what the Cannon provided would be necessary for this. Deposition has historically been modeled as the product of the settling velocity and the near bed concentration, but should also be investigated how the volume available in the contributes to the depositional rates in a plane gravel bed.

In regard to chub spawning nests, a vertical sediment capture distribution would be helpful in determining how much sediment travels to the bottom of the nest versus getting trapped on upper layers of gravel within the nest. Depositional tests within a nest could also be performed in a flume so that the testing environment is more controlled with consistent flow conditions and sediment concentrations present. New sampling jars should be used that have an open front to allow sediment into them in ways other than just from the opening on the top.

With the combination of these two studies, we can confirm that material previously treated as a washload and neglected in transport models, can go through a series of deposition and resuspension phases and should be treated as such.

Bibliography

Bilotta, G. and Brazier, R. (2008). Understanding the influence of suspended solids on water quality and aquatic biota. *Water Research*, 42(12):2849–2861.

Blum, M., Rahn, D., Frederick, B., and Polanco, S. (2023). Land loss in the mississippi river delta: Role of subsidence, global sea-level rise, and coupled atmospheric and oceanographic processes. *Global and Planetary Change*, 222:104048.

Brownlie, W. R. (1981). Prediction of flow depth and sediment discharge in open channels. Report KH-R-43A, W. M. Keck Laboratory of Hydraulics and Water Resources, California Institute of Technology, Pasadena, California, USA.

Buendia, C., Vericat, D., Batalla, R. J., and Gibbins, C. N. (2016). Temporal Dynamics of Sediment Transport and Transient In-channel Storage in a Highly Erodible Catchment. *Land Degradation & Development*, 27(4):1045–1063.

Collins, A. L., Zhang, Y., McMillan, S., Dixon, E. R., Stringfellow, A., Bateman, S., and Sear, D. A. (2017). Sediment-associated organic matter sources and sediment oxygen demand in a special area of conservation (sac): A case study of the river axe, uk. *River Research and Applications*, 33(10):1539–1552.

Culp, J., Parent, A. M., Abolfazli, E., Strom, K., and Romans, B. W. (2021). Advective sorting of silt by currents: A laboratory study. *Sedimentology*, 68(7):3116–3140.

Dallmann, J., Phillips, C. B., Teitelbaum, Y., Saavedra Cifuentes, E. Y., Sund, N., Schumer, R., Arnon, S., and Packman, A. I. (2021). Bedform segregation and locking increase storage of natural and synthetic particles in rivers. *Nature Communications*, 12(1):7315.

Dallmann, J., Phillips, C. B., Teitelbaum, Y., Sund, N., Schumer, R., Arnon, S., and Packman, A. I. (2020). Impacts of suspended clay particle deposition on sand-bed morphodynamics. *Water Resources Research*, 56(8):e2019WR027010.

Dubuis, R. and De Cesare, G. (2023). The clogging of riverbeds: A review of the physical processes. *Earth-Science Reviews*, 239:104374.

Einstein, H. A. (1950). The bed load function for sediment transport in open channels. Technical Bulletin 1026, U.S. Department of Agriculture.

Elliott, A. H. and Brooks, N. H. (1997). Transfer of nonsorbing solutes to a streambed with bed forms: Theory. *Water Resources Research*, 33(1):123–136.

Estrany, J., López-Tarazón, J. A., and Smith, H. G. (2016). Wildfire Effects on Suspended Sediment Delivery Quantified Using Fallout Radionuclide Tracers in a Mediterranean Catchment. *Land Degradation & Development*, 27(5):1501–1512.

Fries, J. S. and Trowbridge, J. H. (2003). Flume observations of enhanced fine-particle deposition to permeable sediment beds. *Limnology and Oceanography*, 48(2):802–812.

Frostick, L. E., Lucas, P. M., and Reid, I. (1984). The infiltration of fine matrices into coarse-grained alluvial sediments and its implications for stratigraphical interpretation. *Journal of the Geological Society*, 141(6):955–965.

Fuller, M. E. (2022). *Determining Incipient Motion Conditions for Mounded Gravel Fish Nests*. Master's Project and Report, Virginia Polytechnic Institute and State University, Blacksburg, Virginia.

Garcia, M. and Parker, G. (1991). Entrainment of Bed Sediment into Suspension. *Journal of Hydraulic Engineering*, 117(4):414–435.

Garcia, M. and Parker, G. (1993). Experiments on the entrainment of sediment into suspension by a dense bottom current. *Journal of Geophysical Research*, 98(3):4793–4807.

García, M. H. (2008). *Sediment Transport and Morphodynamics. Sedimentation Engineering*, chapter 2 Sediment Transport and Morphodynamics, pages 21–163. ASCE Manuals and Reports on Engineering Practice No. 110. ASCE.

Gauthier, V., Barbeau, B., Tremblay, G., Millette, R., and Bernier, A.-M. (2003). Impact of raw water turbidity fluctuations on drinking water quality in a distribution system. *Journal of Environmental Engineering and Science*, 2(4):281–291.

Gupta, L. K., Pandey, M., Raj, P. A., and Shukla, A. K. (2023). Fine sediment intrusion and its consequences for river ecosystems: A review. *Journal of Hazardous, Toxic, and Radioactive Waste*, 27(1).

Hamilton, W. (1971). Geometry for the selfish herd. *Journal of Theoretical Biology*, 31:295–311.

Harvey, J. W., Drummond, J. D., Martin, R. L., McPhillips, L. E., Packman, A. I., Jerolmack, D. J., Stonedahl, S. H., Aubeneau, A. F., Sawyer, A. H., Larsen, L. G., and Tobias, C. R. (2012). Hydrogeomorphology of the hyporheic zone: Stream solute and fine particle interactions with a dynamic streambed. *Journal of Geophysical Research: Biogeosciences*, 117(G4):2012JG002043.

Henderson, F. M. (1966). *Open Channel Flow*. Macmillan Publishing Co.

Hester, E. T., Young, K. I., and Widdowson, M. A. (2013). Mixing of surface and groundwater induced by riverbed dunes: Implications for hyporheic zone definitions and pollutant reactions. *Water Resources Research*, 49(9):5221–5237.

Janssen, F., Cardenas, M. B., Sawyer, A. H., Dammrich, T., Krietsch, J., and Beer, D. (2012). A comparative experimental and multiphysics computational fluid dynamics study of coupled surface–subsurface flow in bed forms. *Water Resources Research*, 48(8):W08514.

Jensen, D. W., Steel, E. A., Fullerton, A. H., and Pess, G. R. (2009). Impact of Fine Sediment on Egg-To-Fry Survival of Pacific Salmon: A Meta-Analysis of Published Studies. *Reviews in Fisheries Science*, 17(3):348–359.

Johnston, C. (1994). The benefit to some minnows of spawning in the nests of other species. *Environmental Biology of Fishes*, 40:213–218.

Kostaschuk, R., Shugar, D., Best, J., Parsons, D., Lane, S., Hardy, R., and Orfeo, O. (2009). Suspended sediment transport and deposition over a dune: Río paraná, argentina. *Earth Surface Processes and Landforms*, 34(12):1605–1611.

Krishnappan, B. . G. . and Engel, P. . (2006). Entrapment of fines in coarse sediment beds. In Alves, E. C., Cardoso, A. H., Leal, J. G., and Ferreira, R. M., editors, *River Flow 2006*, pages 817–824. Taylor & Francis.

Lamb, M. P. and Venditti, J. G. (2016). The grain size gap and abrupt gravel-sand transitions in rivers due to suspension fallout. *Geophysical Research Letters*, 43(8):3777–3785.

Lane, S. N., Bakker, M., Costa, A., Girardclos, S., Loizeau, J.-L., Molnar, P., Silva, T., Stutenbecker, L., and Schlunegger, F. (2019). Making stratigraphy in the Anthropocene: climate change impacts and economic conditions controlling the supply of sediment to Lake Geneva. *Scientific Reports*, 9(1):8904.

Li, D., Li, Z., Zhou, Y., and Lu, X. (2020). Substantial Increases in the Water and Sediment Fluxes in the Headwater Region of the Tibetan Plateau in Response to Global Warming. *Geophysical Research Letters*, 47(11):e2020GL087745.

Maurakis, E., Woolcott, W., and Sabaj Pérez, M. (1991). Reproductive-behavioral phylogenetics of nocomis species-groups. *American Midland Naturalist*, 126:103.

Mehta, A. J. (2022). *An Introduction to Hydraulics of Fine Sediment Transport*, volume Volume 56 of *Advanced Series on Ocean Engineering*. World Scientific.

Mendoza, C. and Shen, H. W. (1990). Investigation of turbulent flow over dunes. *Journal of Hydraulic Engineering*, 116(4).

Mooneyham, C. and Strom, K. (2018a). Deposition of suspended clay to open and sand-filled framework gravel beds in a laboratory flume. *Water Resources Research*, 54:323–344.

Mooneyham, C. and Strom, K. (2018b). Deposition of Suspended Clay to Open and Sand-Filled Framework Gravel Beds in a Laboratory Flume. *Water Resources Research*, 54(1):323–344.

Newcombe, C. P. and Macdonald, D. D. (1991). Effects of Suspended Sediments on Aquatic Ecosystems. *North American Journal of Fisheries Management*, 11(1):72–82.

Osborn, R., Dillon, B., Tran, D., Abolfazli, E., Dunne, K. B. J., Nittrouer, J. A., and Strom, K. (2021). FlocARAZI: An In-Situ, Image-Based Profiling Instrument for Sizing Solid and Flocculated Suspended Sediment. *Journal of Geophysical Research: Earth Surface*, 126(11):e2021JF006210.

Packman, A. I., Brooks, N. H., and Morgan, J. J. (2000). Kaolinite exchange between a stream and streambed: Laboratory experiments and validation of a colloid transport model. *Water Resources Research*, 36(8):2363–2372.

Papanicolaou, A. N., Kramer, C. M., Tsakiris, A. G., Stoesser, T., Bomminayuni, S., and Chen, Z. (2012). Effects of a fully submerged boulder within a boulder array on the mean and turbulent flow fields: Implications to bedload transport. *Acta Geophysica*, 60(6):1502–1546.

Park, J. and Hunt, J. R. (2018). Modeling fine particle dynamics in gravel-bedded streams: Storage and re-suspension of fine particles. *Science of The Total Environment*, 634:1042–1053.

Parker, G. (1990). Surface-based bedload transport relation for gravel rivers. *Journal of Hydraulic Research*, 28(4):417–436.

Partheniades, E. (1977). Unified view of wash load and bed material load. *Journal of the Hydraulics Division*, 103(9):1037–1057.

Peoples, B. K., Tainer, M. B., and Frimpong, E. A. (2011). Bluehead chub nesting activity: a potential mechanism of population persistence in degraded stream habitats. *Environmental Biology of Fishes*, 90(4):379–391.

Potts, G. W., Keenleyside, M. H. A., and Edwards, J. M. (1988). The effect of silt on the parental behaviour of the sea stickleback, spinachia spinachia. *Journal of the Marine Biological Association of the United Kingdom*, 68(2):277–285.

Sanford, L. P. and Maa, J. P. Y. (2001). A unified erosion formulation for fine sediments. *Marine Geology*, 179(1-2):9 – 23.

Schieber, J. and Southard, J. B. (2009). Bedload transport of mud by floccule ripples – direct observation of ripple migration processes and their implications. *Geology*, 37:483–486.

Sear, D. A., Pattison, I., Collins, A. L., Smallman, D. J., Jones, J. I., and Naden, P. S. (2017). The magnitude and significance of sediment oxygen demand in gravel spawning beds for the incubation of salmonid embryos. *River Research and Applications*, 33(10):1642–1654.

Shakeel, A., Zander, F., de Klerk, J.-W., Kirichek, A., Gebert, J., and Chassagne, C. (2022). Effect of organic matter degradation in cohesive sediment: A detailed rheological analysis. *Journal of Soils and Sediments*, 22(11):2883–2892.

Skalak, K. and Pizzuto, J. (2010). The distribution and residence time of suspended sediment stored within the channel margins of a gravel-bed bedrock river. *Earth Surface Processes and Landforms*, 35(4):435–446.

Smith, J. D. and McLean, S. R. (1977). Spatially averaged flow over a wavy surface. *Journal of Geophysical Research*, 82(12):1735–1746.

Smith, S. (2023). Estimating embeddedness from bankfull shear velocity in gravel streambeds to assess sediment impacts on aquatic biota.

Strom, K. and Keyvani, A. (2011). An explicit full-range settling velocity equation for mud flocs. *Journal of Sedimentary Research*, 81(12):921–934.

Strom, K. B. and Papanicolaou, A. N. (2007). ADV measurements around a cluster microform in a shallow mountain stream. *Journal of Hydraulic Engineering*, 133(12):1379–1389.

Tran, D. and Strom, K. (2019). Floc sizes and resuspension rates from fresh deposits: Influences of suspended sediment concentration, turbulence, and deposition time. *Estuarine, Coastal and Shelf Science*, 229:106397.

van Rijn, L. C. (1984). Sediment transport, part iii: Bed forms and alluvial roughness. *Journal of Hydraulic Engineering*, 110(12):1733–1754.

Vives, S. P. (1990). Nesting ecology and behavior of hornyhead chub nocomis biguttatus, a keystone species in allequash creek, wisconsin. *The American Midland Naturalist*, 124(1):46–56.

Wallin, J. E. (1992). The symbiotic nest association of yellowfin shiners, notropis lutipinnis, and bluehead chubs, nocomis leptocephalus. *Environmental Biology of Fishes*, 33:287–292.

Wharton, G., Mohajeri, S. H., and Righetti, M. (2017). The pernicious problem of streambed colmation: a multi-disciplinary reflection on the mechanisms, causes, impacts, and management challenges. *WIREs Water*, 4(5):e1231.

Wiberg, P. L., Law, B. A., Wheatcroft, R. A., Milligan, T. G., and Hill, P. S. (2013). Seasonal variations in erodibility and sediment transport potential in a mesotidal channel-flat complex, willapa bay, {WA}. *Continental Shelf Research*, 60, Supplement(0):S185 – S197.

Wilcock, P. R. (1993). Critical Shear Stress of Natural Sediments. *Journal of Hydraulic Engineering*, 119(4):491–505.

Woo, H. S., Julien, P. Y., and Richardson, E. V. (1986). Washload and Fine Sediment Load. *Journal of Hydraulic Engineering*, 112(6):541–545.

Wright, S. and Parker, G. (2004). Flow resistance and suspended load in sand-bed rivers: Simplified stratification model. *Journal of Hydraulic Engineering*, 130(8):796–805.

Yang, H., Kraus, S., Frimpong, E., Strom, K., and Foroutan, H. (2024). Abstract H14G-07, the impact of bluehead chub nests on near-bed and subsurface flow: Field measurements and 3-D hydrodynamic modeling. In *American Geophysical Union, Fall Meeting 2023*, San Francisco, CA.